
Detecting Misclassification Errors in Neural Networks with a Gaussian Process Model

Xin Qiu¹ Risto Miikkulainen^{1,2}

Abstract

As neural network classifiers are deployed in real-world applications, it is crucial that their failures can be detected reliably. One practical solution is to assign confidence scores to each prediction, then use these scores to filter out possible misclassifications. However, existing confidence metrics are not yet sufficiently reliable for this role. This paper presents a new framework that produces a more reliable quantitative metric for detecting misclassification errors. This framework, RED, builds an error detector on top of the base classifier and estimates uncertainty of the detection scores using Gaussian Processes. Empirical comparisons with other error detection methods on 125 UCI datasets demonstrate that this approach is effective. Additional implementations on two probabilistic base classifiers and a large deep learning architecture solving a vision task further confirm the robustness of the method. A case study involving out-of-distribution and adversarial samples shows potential of the proposed method to improve trustworthiness of neural network classifiers more broadly in the future.

1. Introduction

Classifiers based on Neural Networks (NNs) are widely deployed in many real-world applications (LeCun et al., 2015; Anjos et al., 2015; Alghoul et al., 2018; Shahid et al., 2019). Although good prediction accuracies are achieved, lack of safety guarantees becomes a severe issue when NNs are applied to safety-critical domains, e.g., healthcare (Selişteanu et al., 2018; Gupta et al., 2007; Shahid et al., 2019), finance (Dixon et al., 2017), self-driving (Janai et al., 2017; Hecker et al., 2018), etc.

One way to estimate trustworthiness of a classifier predic-

tion is to use its inherent confidence-related score, e.g., the maximum class probability (Hendrycks & Gimpel, 2017), entropy of the softmax outputs (Williams & Renals, 1997), or difference between the highest and second highest activation outputs (Monteith & Martinez, 2010). However, these scores are unreliable and may even be misleading: high-confidence but erroneous predictions are frequently observed (Provost et al., 1998; Guo et al., 2017; Nguyen et al., 2015; Goodfellow et al., 2014; Amodei et al., 2016). In a practical setting, it is beneficial to have a detector that can raise a red flag whenever the predictions are suspicious. A human observer can then evaluate such predictions, making the classification system safer.

In order to construct such a detector, quantitative metrics for measuring predictive reliability under different circumstances are first developed, and a warning threshold then be set based on users' preferred precision-recall tradeoff. Existing such methods can be categorized into three types based on their focus: error detection, which aims to detect the natural misclassifications made by the classifier (Hendrycks & Gimpel, 2017; Jiang et al., 2018; Corbière et al., 2019); out-of-distribution (OOD) detection, which reports samples that are from different distributions compared to training data (Liang et al., 2018; Lee et al., 2018a; Devries & Taylor, 2018); and adversarial sample detection, which filters out samples from adversarial attacks (Lee et al., 2018b; Wang et al., 2019; Aigrain & Detyniecki, 2019).

Among these categories, error detection, also called misclassification detection (Jiang et al., 2018) or failure prediction (Corbière et al., 2019), is the most challenging (Aigrain & Detyniecki, 2019) and underexplored. For instance, Hendrycks & Gimpel (2017) defined a baseline utilizing maximum class probability after softmax layer as the error detection score. Although the baseline performs reasonably well in most testing cases, reduced efficacy in some scenarios indicates room for improvement (Hendrycks & Gimpel, 2017). Jiang et al. (2018) proposed Trust Score, which measures the similarity between the original classifier and a modified nearest-neighbor classifier. The main limitation of this method is scalability: the Trust Score may provide no or negative improvement over the baseline for high-dimensional data. ConfidNet (Corbière et al., 2019) builds a separate NN model to learn the true class prob-

¹Cognizant, San Francisco, CA, USA ²The University of Texas at Austin, Austin, TX, USA. Correspondence to: Xin Qiu <qixun.nju@gmail.com>, Risto Miikkulainen <risto@cognizant.com>.

ability, i.e. softmax probability for the ground-truth class. However, ConfidNet itself is a standard NN, so its detection scores may be unreliable or misleading: A random input may generate a random detection score, and ConfidNet do not provide any information regarding uncertainty of these detection scores. Moreover, none of these methods can differentiate natural classifier errors from risks caused by OOD or adversarial samples; if a detector could do that, it would be easier for practitioners to fix the problem, e.g., by retraining the original classifier or applying better preprocessing techniques to filter out OOD or adversarial data.

To meet these challenges, a new framework is developed in this paper for error (misclassification) detection in NN classifiers. The main idea is to utilize RIO (Residual, Input, Output; Qiu et al., 2020), a regression model based on Gaussian Processes, on top of the original NN classifier. Whereas the original RIO is limited to regression problems, the proposed approach extends it to error detection in classification problems by modifying its components. The new framework not only produces an error detection score based on the original maximum class probability, but also provides a quantitative uncertainty estimation of that score. Errors can therefore be detected more reliably. Note that the proposed method does not change the outputs of the original classification model. Instead, it provides an additional quantitative metric that makes it possible to detect misclassification errors. This work is also different from those traditional confidence calibration methods (Platt, 1999; Zadrozny & Elkan, 2001, 2002; Guo et al., 2017), in which separability between correct and incorrect predictions is not improved. The proposed framework, referred to as RED (RIO for Error Detection), is compared empirically to existing error detection methods on 125 UCI datasets and a vision task, with implementations on one standard NN classifier, two probabilistic NN classifiers, and a deep NN architecture. The results demonstrate that the approach is effective and robust. A further case study with OOD and adversarial samples shows the potential of using RED to diagnose the sources of mistakes as well, thereby leading to a possible comprehensive approach for improving trustworthiness of neural network classifiers in the future.

2. Related Work

In the past two decades, a large volume of work was devoted to calibrating the confidence scores returned by classifiers. Early works include Platt Scaling (Platt, 1999; Niculescu-Mizil & Caruana, 2005), histogram binning (Zadrozny & Elkan, 2001), isotonic regression (Zadrozny & Elkan, 2002), with recent extensions like Temperature Scaling (Guo et al., 2017), Dirichlet calibration (Kull et al., 2019), and distance-based learning from errors (Xing et al., 2020). These methods focus on reducing the difference between reported class probability and true accuracy, and generally the rankings

of samples are preserved after calibration. As a result, the separability between correct and incorrect predictions is not improved. In contrast, RED aims at deriving a score that can differentiate incorrect predictions from correct ones better.

A related direction of work is the development of classifiers with rejection/abstention option. These approaches either introduce new training pipelines/loss functions (Bartlett & Wegkamp, 2008; Yuan & Wegkamp, 2010; Cortes et al., 2016), or define mechanisms for learning rejection thresholds under certain risk levels (Dubuisson & Masson, 1993; Santos-Pereira & Pires, 2005; Chow, 2006; Geifman & El-Yaniv, 2017). In contrast to these methods, RED assumes an existing pretrained NN classifier, and provides an additional metric for detecting potential errors made by this classifier, without specifying a rejection threshold.

Designing metrics for detecting potential risks in NN classifiers has also become popular recently. While most approaches focus on detecting OOD (Liang et al., 2018; Lee et al., 2018a; Devries & Taylor, 2018) or adversarial examples (Lee et al., 2018b; Wang et al., 2019; Aigrain & Detyniecki, 2019), work on detecting natural errors, i.e., regular misclassifications not caused by external sources, is more limited. Ortega (1995) and Koppel & Engelson (1996) conducted early work in predicting whether a classifier is going to make mistakes, and Seewald & Fürnkranz (2001) built a meta-grading classifier based on similar ideas. However, these early works did not consider NN classifiers. More recently, Hendrycks & Gimpel (2017) and Haldimann et al. (2019) demonstrated that raw maximum class probability is an effective baseline in error detection, although its performance was reduced in some scenarios. More elaborate techniques for error detection have also been developed recently. Mandelbaum & Weinshall (2017) proposed a detection score based on the data embedding derived from the penultimate layer of a NN. However, their approach requires modifying the training procedure in order to achieve effective embeddings. Jiang et al. (2018) introduced Trust Score to measure the similarity between a base classifier and a modified nearest-neighbor classifier. Trust Score outperforms the maximum class probability baseline in many cases, but negative improvement over baseline can be observed in high-dimensional problems, implying poor scalability of local distance computations. ConfidNet (Corbière et al., 2019) learns to predict the class probability of true class with another NN, while Introspection-Net (Aigrain & Detyniecki, 2019) utilizes the logit activations of the original NN classifier to predict its correctness. Since both models themselves are standard NNs, the detection scores returned by them may be arbitrarily high without any uncertainty information. Moreover, existing approaches for error detection cannot differentiate natural misclassification error from OOD or adversarial samples, making it difficult to diagnose the sources of risks. In contrast, RED explicitly reports its

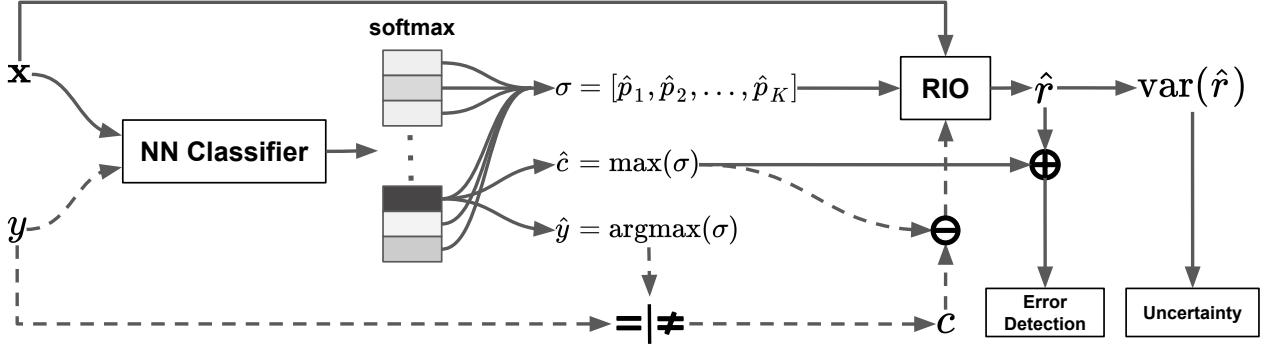


Figure 1. The RED Training and Deployment Processes. The solid pathways are active in both training and deployment phase, while the dashed pathways are active only in the training phase. During the training phase, a target detection score c is assigned to each training sample according to whether it is correctly predicted by the original NN classifier or not. A RIO model is then trained to predict the residual between the target detection score c and the original maximum class probability \hat{c} . The I/O kernel in RIO utilizes both the raw feature \mathbf{x} and softmax outputs σ to predict the residuals. In the deployment phase, given a new data point, the trained RIO model provides a Gaussian distribution of estimated residual \hat{r} defined by the mean \bar{r} and variance $\operatorname{var}(\hat{r})$. Addition of \hat{r} and \hat{c} forms a score for error detection, and $\operatorname{var}(\hat{r})$ indicates the corresponding uncertainty.

uncertainty about the estimated detection score, providing more reliable error detection. The uncertainty information returned by RED may also be helpful in clarifying the cause of classifier mistakes, as will be demonstrated in this paper.

3. Methodology

This section gives the general problem statement, introduces the basic idea of original RIO, on which RED is built, and describes the technical details of RED.

3.1. Problem Statement

Consider a training dataset $\mathcal{D} = (\mathcal{X}, \mathbf{y}) = \{(\mathbf{x}_i, y_i)\}_{i=1}^N$, and a pretrained NN classifier that outputs a predicted label \hat{y}_i and class probabilities for each class $\sigma_i = [\hat{p}_{i,1}, \hat{p}_{i,2}, \dots, \hat{p}_{i,K}]$ given \mathbf{x}_i , where N is the total number of training points and K is the total number of classes. The problem is to develop a metric that can serve as a quantitative indicator for detecting natural misclassification errors made by the pretrained NN classifier.

3.2. RIO

The original RIO (Qiu et al., 2020) was developed to quantify point-prediction uncertainty in regression models. More specifically, RIO fits a Gaussian Process (GP) to predict the residuals, i.e. the differences between ground-truth and original model predictions. It utilizes an I/O kernel, i.e. a composite of an input kernel and an output kernel, thus taking into account both inputs and outputs of the original regression model. As a result, it measures the covariances between data points in both the original feature space and the original model output space. For each new data point,

a trained RIO model takes the original input and output of the base regression model, and predicts a distribution of the residual, which can be added back to the original model prediction to obtain both a calibrated prediction and the corresponding predictive uncertainty.

In the original RIO work, SVGP (Hensman et al., 2013; 2015) was used as an approximate GP to significantly reduce the computational cost. Both empirical results and theoretical analysis showed that RIO is able to consistently improve the prediction accuracy of base model as well as provide reliable uncertainty estimation. Moreover, RIO can be directly applied on top of any pre-trained models without retraining or modification. It therefore forms a promising foundation for improving reliability of error detection metrics as well.

3.3. RIO for Error Detection (RED)

Although RIO performs robustly in a wide variety of regression problems, it cannot be directly applied to classification models. A new framework, namely RED, is proposed to utilize RIO for error detection in classification domains.

Building on the fact that the original maximum class probability is a strong baseline for error detection (Hendrycks & Gimpel, 2017; Haldimann et al., 2019), the main idea of RED is to derive a more reliable detection score by stacking RIO on top of the original maximum class probability. Since RIO was designed for single-output regression problems, it contains an output kernel only for scalar outputs. In RED, this original output kernel is extended to multiple outputs, i.e. to vector outputs such as those of the final softmax layer of a NN classifier, representing estimated class probabilities

Algorithm 1 RED Training and Deployment Procedures

Require:

- $(\mathcal{X}, \mathbf{y}) = \{(\mathbf{x}_i, y_i)\}_{i=1}^N$: training data
 $\hat{\mathbf{y}} = \{\hat{y}_i\}_{i=1}^N$: labels predicted by original NN classifier on training data
 $\boldsymbol{\sigma} = \{\sigma_i = [\hat{p}_{i,1}, \hat{p}_{i,2}, \dots, \hat{p}_{i,K}]\}_{i=1}^N$: softmax outputs of original NN classifier on training data
 $\hat{\mathbf{c}} = \{\hat{c}_i = \max(\sigma_i)\}_{i=1}^N$: maximum class probability returned by original NN classifier on training data
 \mathbf{x}_* : data to be predicted
 σ_* : softmax outputs of original NN classifier on \mathbf{x}_*
 \hat{c}_* : maximum class probability returned by original NN classifier on \mathbf{x}_*

Ensure:

- $\hat{c}'_* \sim \mathcal{N}(\hat{c}_* + \bar{r}_*, \text{var}(\hat{r}_*))$: $\hat{c}_* + \bar{r}_*$ can be used as detection score for error detection, and $\text{var}(\hat{r}_*)$ represents the uncertainty of returned detection score

Training Phase:

- 1: obtain target detection score $\mathbf{c} = \{c_i = \delta_{y_i, \hat{y}_i}\}_{i=1}^N$, where δ_{y_i, \hat{y}_i} is the Kronecker delta ($\delta_{y_i, \hat{y}_i} = 1$ if $y_i = \hat{y}_i$, otherwise $\delta_{y_i, \hat{y}_i} = 0$)
- 2: calculate residuals $\mathbf{r} = \{r_i = c_i - \hat{c}_i\}_{i=1}^N$
- 3: **for** each optimizer step **do**
- 4: calculate covariance matrix $\mathbf{K}_c((\mathcal{X}, \boldsymbol{\sigma}), (\mathcal{X}, \boldsymbol{\sigma}))$, where each entry is given by $k_c((\mathbf{x}_i, \sigma_i), (\mathbf{x}_j, \sigma_j)) = k_{\text{in}}(\mathbf{x}_i, \mathbf{x}_j) + k_{\text{out}}(\sigma_i, \sigma_j)$, for $i, j = 1, 2, \dots, N$
- 5: optimize GP hyperparameters by maximizing log marginal likelihood $\log p(\mathbf{r}|\mathcal{X}, \boldsymbol{\sigma}) = -\frac{1}{2}\mathbf{r}^\top (\mathbf{K}_c((\mathcal{X}, \boldsymbol{\sigma}), (\mathcal{X}, \boldsymbol{\sigma})) + \sigma_n^2 \mathbf{I})^{-1} \mathbf{r} - \frac{1}{2} \log |\mathbf{K}_c((\mathcal{X}, \boldsymbol{\sigma}), (\mathcal{X}, \boldsymbol{\sigma})) + \sigma_n^2 \mathbf{I}| - \frac{n}{2} \log 2\pi$

Deployment Phase:

- 6: calculate residual mean $\bar{r}_* = \mathbf{k}_*^\top (\mathbf{K}_c((\mathcal{X}, \boldsymbol{\sigma}), (\mathcal{X}, \boldsymbol{\sigma})) + \sigma_n^2 \mathbf{I})^{-1} \mathbf{r}$ and residual variance $\text{var}(\hat{r}_*) = k_c(\mathbf{x}_*, \sigma_*, \mathbf{x}_*, \sigma_*) - \mathbf{k}_*^\top (\mathbf{K}_c((\mathcal{X}, \boldsymbol{\sigma}), (\mathcal{X}, \boldsymbol{\sigma})) + \sigma_n^2 \mathbf{I})^{-1} \mathbf{k}_*$, where \mathbf{k}_* denotes the vector of kernel-based covariances (i.e., $k_c(\mathbf{x}_*, \mathbf{x}_i)$) between \mathbf{x}_* and all the training points
- 7: return distribution of error detection score $\hat{c}'_* \sim \mathcal{N}(\hat{c}_* + \bar{r}_*, \text{var}(\hat{r}_*))$

for each class. This modification allows RIO to access more information from the classifier outputs.

The targets for RIO training need to be redesigned as well. The raw targets of a classification problem are the ground-truth labels; they are in categorical space, while RIO works in continuous space. To solve this issue, RED constructs a different problem: Instead of predicting the labels directly, it predicts whether the original prediction is correct or not. A target detection score is assigned to each training data point accordingly. The residual between this target score and the originally returned maximum class probability is calculated, and a RIO model is trained to predict these residuals. Given a new data point, the trained RIO model combined with the original NN classifier thus provides an aggregated score for detecting misclassification errors.

Figure 1 illustrates the RED training and deployment processes conceptually, and Algorithm 1 specifies them in detail. In the training phase, the first step is to define a target detection score c_i for each training sample $(\mathbf{x}_i, y_i, \hat{y}_i, \sigma_i)$. In nature, any functions that assign target values to correct and incorrect predictions differently can be used. For simplicity, the Kronecker delta δ_{y_i, \hat{y}_i} is used in this work: all training samples that are correctly predicted by the original NN classifier receive 1 as the target detection score, and those that are incorrectly predicted receive 0. The validation

dataset during the original NN training is included in the training dataset for RED. After the target detection scores are assigned, a regression problem is formulated for the RIO model: Given the original raw features $\{\mathbf{x}_i\}_{i=1}^N$ and the corresponding softmax outputs of the original NN classifier $\{\sigma_i = [\hat{p}_{i,1}, \hat{p}_{i,2}, \dots, \hat{p}_{i,K}]\}_{i=1}^N$, predict the residuals $\mathbf{r} = \{r_i = c_i - \hat{c}_i\}_{i=1}^N$ between target detection scores $\mathbf{c} = \{c_i\}_{i=1}^N$ and the original maximum class probabilities $\hat{\mathbf{c}} = \{\hat{c}_i = \max(\sigma_i)\}_{i=1}^N$.

The RIO model relies on an I/O kernel consisting of two components: the input kernel $k_{\text{in}}(\mathbf{x}_i, \mathbf{x}_j)$, which measures covariances in the raw feature space, and the modified multi-output kernel $k_{\text{out}}(\sigma_i, \sigma_j)$, which calculates covariances in the softmax output space. The hyperparameters of the I/O kernel are optimized to maximize the log marginal likelihood $\log p(\mathbf{r}|\mathcal{X}, \boldsymbol{\sigma})$. In the deployment phase, given a new data point \mathbf{x}_* , the trained RIO model provides a Gaussian distribution for the estimated residual $\hat{r}_* \sim \mathcal{N}(\bar{r}_*, \text{var}(\hat{r}_*))$. By adding the estimated residual back to the original maximum class probability \hat{c}_* , a distribution of detection score is obtained as $\hat{c}'_* \sim \mathcal{N}(\hat{c}_* + \bar{r}_*, \text{var}(\hat{r}_*))$. The mean $\hat{c}_* + \bar{r}_*$ can be directly used as a quantitative metric for error detection, and the variance $\text{var}(\hat{r}_*)$ represents the corresponding uncertainty of the detection score.

Table 1. Mean Rank on UCI datasets

Method	AP-Error mean±std	AUPR-Error mean±std	AP-Success mean±std	AUPR-Success mean±std	AUROC mean±std
RED	1.39±0.61*	1.49±0.78*	1.74±0.97*	1.80±1.03*	1.65±0.82*
MCP Baseline	2.93±0.89	3.06±0.92	2.77±1.07	2.75±1.11	2.80±1.08
Trust Score	3.92±2.45	3.86±2.50	3.64±2.25	3.61±2.25	3.76±2.31
ConfidNet	6.13±1.37	6.33±1.38	6.07±1.51	6.07±1.41	5.97±1.45
Introspection-Net	5.34±1.65	5.38±1.65	5.83±1.46	5.89±1.51	5.71±1.50
Entropy	3.47±1.08	3.59±1.19	3.19±1.26	3.23±1.32	3.26±1.28
DNGO	6.19±1.51	5.46±1.82	6.84±1.33	6.80±1.44	6.57±1.47
SVGP	6.59±1.60	6.80±1.49	5.89±1.54	5.83±1.49	6.24±1.61

The symbols * indicates that the differences between the marked entry and all other counterparts are statistically significant at the 5% significance level for both paired t -test and Wilcoxon test. The best entries that are significantly better than all the others under both statistical test are marked in boldface.

Table 2. A Pairwise Comparison between RED and Other Methods on UCI datasets

Method	AP-Error + / = / -	AUPR-Error + / = / -	AP-Success + / = / -	AUPR-Success + / = / -	AUROC + / = / -
MCP Baseline	87 / 35 / 0	90 / 32 / 0	58 / 63 / 1	56 / 65 / 1	61 / 60 / 1
Trust Score	53 / 44 / 16	49 / 47 / 17	50 / 47 / 16	48 / 49 / 16	59 / 37 / 17
ConfidNet	100 / 22 / 0	100 / 22 / 0	106 / 16 / 0	106 / 16 / 0	109 / 13 / 0
Introspection-Net	93 / 29 / 0	90 / 32 / 0	98 / 24 / 0	98 / 24 / 0	101 / 21 / 0
Entropy	74 / 47 / 1	75 / 46 / 1	53 / 68 / 1	53 / 68 / 1	52 / 69 / 1
DNGO	92 / 17 / 0	73 / 31 / 5	99 / 10 / 0	97 / 12 / 0	98 / 11 / 0
SVGP	98 / 23 / 1	98 / 23 / 1	97 / 25 / 0	97 / 25 / 0	102 / 19 / 1

The columns labeled + show the number of datasets on which RED performs significantly better at the 5% significance level in a paired t -test, Wilcoxon test, or both; those labeled - represent the contrary case; those labeled = represent no statistical significance.

4. Empirical Evaluation

In this section, the error detection performance of RED is evaluated comprehensively on 125 UCI datasets, comparing it to other related methods. Its generality is then evaluated by applying it to two other base models, and its scale-up properties measured in a larger deep learning architecture solving a vision task. Finally, RED’s potential to improve robustness more broadly is demonstrated in a case study involving OOD and adversarial samples.

4.1. Comparisons with Related Approaches

As a comprehensive evaluation of RED, an empirical comparison with seven related approaches on 125 UCI datasets (Dua & Graff, 2017) was performed. These approaches include maximum class probability baseline (MCP; Hendrycks & Gimpel, 2017), three state-of-the-art approaches, namely Trust Score (Jiang et al., 2018), ConfidNet (Corbière et al., 2019), and Introspection-Net (Aigrain & Detyniecki, 2019), as well as three earlier approaches, i.e. entropy of the original softmax outputs (Steinhardt & Liang, 2016), DNGO (Snoek et al., 2015), and the original SVGP (Hensman et al., 2013; 2015). The 125 UCI datasets include 121 datasets used by Klambauer et al. (2017) and four more recent ones. Full details about the datasets and parametric setup of all tested algorithms, and a downloadable link for source codes are provided in Appendix A.1.

Following the experimental setup of Hendrycks & Gimpel (2017); Corbière et al. (2019); Aigrain & Detyniecki (2019), the task for each algorithm is to provide a detection score for each testing point. An error detector can then use a predefined fixed threshold on this score to decide which points are probably misclassified by the original NN classifier. For RED, the mean $\hat{c}_* + \bar{r}_*$ was used as the reported detection score. Five threshold-independent performance metrics were used to compare the methods: AUPR-Error, which computes the area under the Precision-Recall (AUPR) Curve when treating incorrect predictions as positive class during the detection; AUPR-Success, which is similar to AUPR-Error but uses correct predictions as positive class; AUROC, which computes the area under receiver operating characteristic (ROC) curve for the error detection task; AP-Error, which computes the average precision (AP) under different thresholds treating incorrect predictions as positive class; and AP-Success, which is similar to AP-Error but uses correct predictions as positive class. AUPR and AUROC are commonly used in prior work (Hendrycks & Gimpel, 2017; Corbière et al., 2019; Aigrain & Detyniecki, 2019), but as discussed by Davis & Goadrich (2006) and Flach & Kull (2015), AUPR may provide overly-optimistic measurement of performance. Moreover, AUROC is sometimes less informative (Manning & Schütze, 1999) and not ideal when the positive class and negative class have greatly differing base rates (Hendrycks & Gimpel, 2017) (this happens when the base classifier has high prediction accuracy so there are

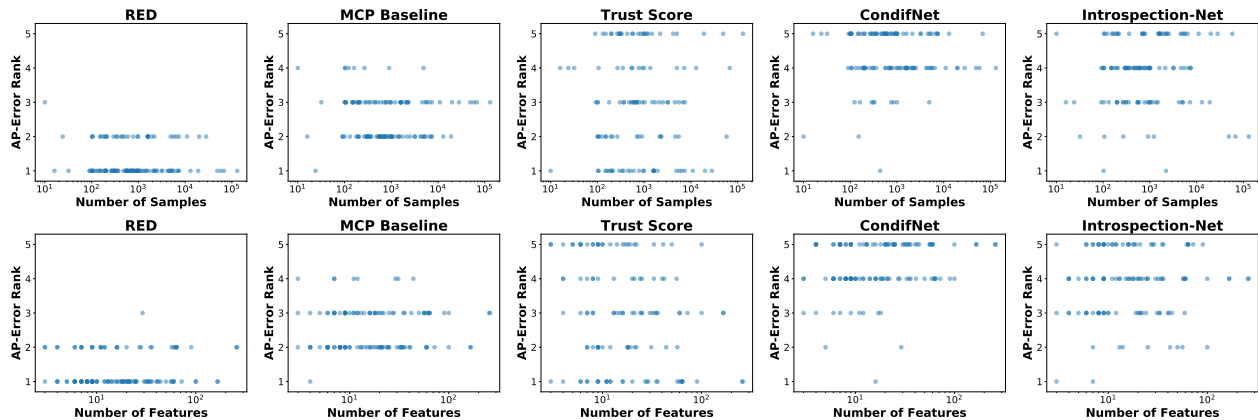


Figure 2. Performance Ranks Across Dataset Sizes and Dimensionalities on UCI Datasets. Each plot represents the distribution of relative ranks for one method (each column) as a function of the dataset size (top row) and the feature dimensionality (bottom row). Each dot in each plot represents the relative rank in one dataset. RED performs consistently well over datasets of different sizes and dimensionalities. Trust Score performs inconsistently, and ConfidNet performs poorly on larger datasets.

only few misclassified examples). To compensate for this issue, AP-Error and AP-Success are included as additional metrics. Since the target of all tested approaches is to detect misclassification errors, the following discussion will focus more on AP-Error and AUPR-Error.

Ten independent runs were conducted for each dataset. During each run, the dataset was randomly split into training dataset and testing dataset, and a standard NN classifier trained and evaluated on them. The same dataset split and trained NN classifier were used to evaluate all methods. The testbed covers a diversified collection of dataset sizes and classifier accuracies, thereby enabling a comprehensive evaluation of the tested approaches. Full details of the experimental setup are provided in Section A.1.

Table 1 shows the ranks of each algorithm averaged over all 125 UCI datasets (detailed results for each individual dataset are provided in Section A.3). The rank of each algorithm on each dataset is based on the average performance over 10 independent runs. RED performs best on all metrics; the performance differences between RED and all other methods are statistically significant under paired t -test and Wilcoxon test. Trust Score has the highest standard deviation, suggesting that its performance varies significantly across different datasets.

As a more detailed comparison, Table 2 shows how often RED performs statistically significantly better, how often the performance is not significantly different, and how often it performs significantly worse than the other methods. RED is most often significantly better, and very rarely worse. In a handful of datasets Trust Score is better, but most often it is not.

To illustrate the performance of RED further compared to

the baseline and the three state-of-the-art approaches, Figure 2 shows the distribution of the relative rank of RED, MCP baseline, Trust Score, ConfidNet and Introspection-Net as a function of the number of samples and the number of features in the dataset. These plots are based on the AP-Error metric; other metrics provide similar results. RED performs consistently well over different dataset sizes and feature dimensionalities. Trust Score performs best in several datasets, but occasionally also worst in both small and large datasets, making it a rather unreliable choice. ConfidNet generally exhibits worse performance on datasets with large dataset sizes and high feature dimensionalities, i.e. it does not scale well to larger problems.

4.2. Generality wrt. Base Models

To evaluate generality and robustness of RED, it was applied to two other base models: an NN classifier using MC-dropout technique (Gal & Ghahramani, 2016) and a Bayesian Neural Network (BNN) classifier (Wen et al., 2018). They were each trained as base classifiers, and RED was then applied to each of them (implementation details are provided in Section A.1). Experiments analogous to those in Table 2 were performed on 125 UCI datasets in both cases. Table 3 shows the pairwise comparisons between RED and the internal detection scores returned by the base models (detailed results for each individual dataset are provided in Section A.3). MCP and Entropy represent the maximum class probability and entropy of softmax outputs, respectively, after averaging over 100 test-time samplings. RED significantly improves MC-dropout and BNN classifier in most datasets, demonstrating that it is a general technique that can be applied to a variety of models.

Table 3. A Pairwise Comparison between RED and Other Methods on UCI datasets

Method	AP-Error + / = / -	AUPR-Error + / = / -	AP-Success + / = / -	AUPR-Success + / = / -	AUROC + / = / -
BNN MCP	102 / 20 / 0	104 / 18 / 0	95 / 26 / 1	88 / 33 / 1	95 / 26 / 1
BNN Entropy	67 / 53 / 2	68 / 52 / 2	48 / 66 / 8	48 / 66 / 8	53 / 64 / 5
MC-Dropout MCP	87 / 35 / 0	88 / 34 / 0	70 / 52 / 0	67 / 55 / 0	71 / 51 / 0
MC-Dropout Entropy	54 / 68 / 0	55 / 67 / 0	38 / 77 / 7	38 / 76 / 8	42 / 74 / 6

The columns labeled + show the number of datasets on which RED performs significantly better at the 5% significance level in a paired *t*-test, Wilcoxon test, or both; those labeled - represent the contrary case; those labeled = represent no statistical significance.

Table 4. A Comparison based on the VGG16 Network Architecture on the CIFAR-10 Task

Metric	RED mean±std	MCP Baseline mean±std	Trust Score mean±std	ConfidNet mean±std	Introspection-Net mean±std	Entropy mean±std	DNGO mean±std	SVGP mean±std
AP-Error(%)	49.88±1.99*	47.09±2.19	48.76±2.28	45.80±2.85	42.11±1.98	47.91±2.17	33.91±2.94	40.71±2.33
AUPR-Error(%)	49.79±2.00*	46.99±2.21	48.68±2.29	45.70±2.86	42.01±1.98	47.81±2.19	34.43±2.92	40.60±2.34

The symbols * indicates that the differences between the marked entry and all other counterparts are statistically significant at the 5% significance level for both paired *t*-test and Wilcoxon test. The best entries that are significantly better than all the others under both statistical test are marked in boldface.

4.3. Scaling up to Larger Architectures

To confirm that the RED approach scales up to large deep learning architectures, a VGG16 model (Simonyan & Zisserman, 2015) was trained on the CIFAR-10 dataset using a state-of-the-art training pipeline (see Section A.2). In order to remove the influence of feature extraction in image preprocessing and to make the comparison fair, all approaches used the same logit outputs of the trained VGG16 model as their input features. 10 independent runs are performed. During each run, a VGG16 model is trained, and all the methods are evaluated based on this VGG16 model.

Table 4 shows the results on the two main error detection performance metrics (note that the table lists absolute values instead of rankings along each metric). Trust Score performs much better than in previous literatures (Corbière et al., 2019). This difference may be due to the fact that logit outputs are used as input features here, whereas Corbière et al. (2019) utilized a higher dimensional feature space for Trust Score. Based on the results, RED significantly outperforms all the counterparts in both metrics. This result demonstrates the advantages of RED in scaling up to larger architectures.

4.4. A Case Study with OOD and Adversarial Samples

In all experiments so far, the mean of detection score $\hat{c}_* + \bar{\hat{r}}_*$ was used as RED’s detection metric. Although good performance is observed in error detection by only using the mean, the variance of detection score $\text{var}(\hat{r}_*)$ may be helpful if the scenario is more complex, e.g., the dataset includes some OOD data, or even adversarial data. A preliminary investigation of RED in such scenarios was performed by manually adding OOD and adversarial data into the test set of the UCI “annealing” dataset, on which RED detected errors well. The synthetic OOD and adversarial samples

were created to be highly deceptive, aiming to evaluate the performance of RED under difficult circumstances. The OOD data were sampled from a Gaussian distribution with mean 0 and variance 1, and the number of added OOD data was the same as the number of samples in the original test set. Note that all data points from original dataset are normalized to have mean 0 and variance 1 for each feature dimension during preprocessing, so the OOD data and in-distribution data have similar scales. The adversarial data was created by adding negligible modifications to training samples that the original NN classifier predicted incorrectly with highest confidence. This process mimics an adversary that can arbitrarily alter the output of the NN classifier with minuscule changes to the input (Goodfellow et al., 2014).

Figure 3 shows the distribution of mean and variance of detection scores for testing samples, including correctly and incorrectly labeled actual samples, as well as the synthetic OOD and adversarial samples. The mean is a good separator for correctly classified and incorrectly classified samples, which tend to cluster on the top and bottom half of the image, respectively. On the other hand, variance is a promising indicator of OOD and adversarial samples. RED’s detection scores of in-distribution samples have low variance because they covary with the training samples. The variance thus represents RED’s confidence in its detection score. Samples with large variance indicate that RED is uncertain about its detection score, which can be used as a basis for detecting OOD and adversarial samples.

Thus, although the main focus of this paper is to demonstrate RED on misclassification detection, the preliminary results in this subsection show that it provides a promising foundation for detecting other error types as well.

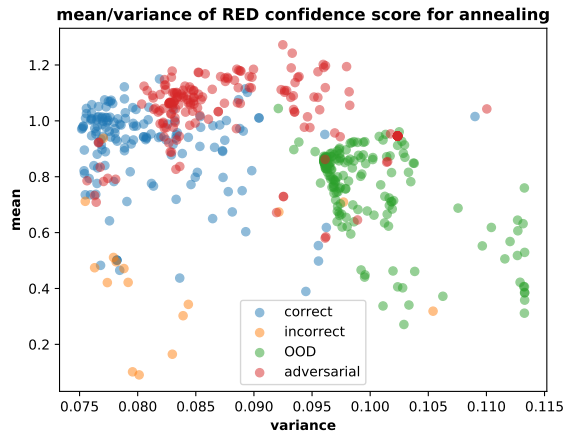


Figure 3. Identifying OOD and Adversarial Samples Based on Mean and Variance of detection Scores. Each dot represents one sample in the testing set in the UCI Annealing task. The horizontal axis denotes the variance of RED-returned detection score, and the vertical axis denotes the mean. If an in-distribution sample is correctly classified by original NN classifier, it is marked as "correct", otherwise it is marked "incorrect". Mean is a good separator of correct and incorrect classifications. High variance, on the other hand, indicates that RED is uncertain about its detection score, which can be used to identify OOD and adversarial samples. In this manner, RED can serve as a foundation for improving robustness of classifiers more broadly in the future.

5. Discussion and Future Work

One interesting observation from the experiments is that RED almost never performs worse than the MCP baseline. This result suggests that there is almost no risk in applying RED on top of an existing NN classifier. Since RED is based on a GP model, the estimated residual $\hat{\epsilon}_*$ is close to zero if the predicted sample is far from the distribution of the original training samples, resulting in no change to the original MCP. In other words, RED does not make random changes to original MCP if it is very uncertain about the predicted sample, and this uncertainty is explicitly represented in the variance of the estimated detection score. This property makes RED a particularly reliable technique for error detection.

Another interesting observation is that the variance is also helpful in detecting OOD and adversarial samples. This result follows from the design of the RIO uncertainty model. Since RIO in RED has an input kernel and an output kernel, lower estimated variance requires that the predicted sample is close to training samples in both the input feature space and the classifier output space. This requirement is difficult for OOD and adversarial attacks to achieve, providing a basis for detecting them.

The most compelling direction of future work is to extend this capability of RED further. Instead of using a single

dimensional score for error detection, it is possible to use mean and variance simultaneously, leading to a two dimensional detection space. Further separation between OOD and adversarial samples may be possible by adding one more dimension, such as the ratio between input kernel output and output kernel output. Also, instead of using a hard target detection score (i.e. either 0 or 1), it may be possible to define a soft target score that may be more informative. Further, RED may be used on top of other existing detection metrics, such as the Trust Score, which may lead to a further improvement in detection performance.

6. Conclusion

This paper introduced a new framework, RED, for error detection in neural network classifiers that can produce a more reliable detection score than previous methods. RED is able to not only provide a detection score, but also report the uncertainty of that score. Experimental results show that RED's scores consistently outperform state-of-the-art methods in separating the misclassified samples from correctly classified samples. Further empirical studies also demonstrate that the approach is applicable to various types of base classifiers, scales up to large deep learning architectures, and can form a basis for detecting OOD and adversarial samples as well. It is therefore a promising foundation for improving robustness of neural network classifiers.

References

- Aigrain, J. and Detyniecki, M. Detecting adversarial examples and other misclassifications in neural networks by introspection. *CoRR*, abs/1905.09186, 2019. URL <http://arxiv.org/abs/1905.09186>.
- Alghoul, A., Ajrami, S. A., Jarousha, G. A., Harb, G., and Abu-Naser, S. S. Email classification using artificial neural network. *International Journal of Academic Engineering Research (IJAER)*, 2(11):8–14, 2018.
- Amodei, D., Olah, C., Steinhardt, J., Christiano, P., Schulman, J., and Mané, D. Concrete problems in ai safety. 06 2016.
- Anjos, O., Iglesias, C., Peres, F., Martínez, J., García, A., and Taboada, J. Neural networks applied to discriminate botanical origin of honeys. *Food Chemistry*, 175:128 – 136, 2015. ISSN 0308-8146. doi: <https://doi.org/10.1016/j.foodchem.2014.11.121>. URL <http://www.sciencedirect.com/science/article/pii/S0308814614018597>.
- Bartlett, P. L. and Wegkamp, M. H. Classification with a reject option using a hinge loss. *J. Mach. Learn. Res.*, 9: 1823–1840, June 2008. ISSN 1532-4435.

- Chow, C. On optimum recognition error and reject trade-off. *IEEE Trans. Inf. Theor.*, 16(1):41–46, September 2006. ISSN 0018-9448. doi: 10.1109/TIT.1970.1054406. URL <https://doi.org/10.1109/TIT.1970.1054406>.
- Corbière, C., THOME, N., Bar-Hen, A., Cord, M., and Pérez, P. Addressing failure prediction by learning model confidence. In *Advances in Neural Information Processing Systems 32*, pp. 2902–2913. Curran Associates, Inc., 2019.
- Cortes, C., DeSalvo, G., and Mohri, M. Learning with rejection. In *Algorithmic Learning Theory*, pp. 67–82, Cham, 2016. Springer International Publishing. ISBN 978-3-319-46379-7.
- Davis, J. and Goadrich, M. The relationship between precision-recall and roc curves. volume 06, 06 2006. doi: 10.1145/1143844.1143874.
- Devries, T. and Taylor, G. W. Learning confidence for out-of-distribution detection in neural networks. *ArXiv*, abs/1802.04865, 2018.
- Dixon, M., Klabjan, D., and Bang, J. Classification-based financial markets prediction using deep neural networks. *Algorithmic Finance*, 12 2017. doi: 10.2139/ssrn.2756331.
- Dua, D. and Graff, C. UCI machine learning repository, 2017. URL <http://archive.ics.uci.edu/ml>.
- Dubuisson, B. and Masson, M. A statistical decision rule with incomplete knowledge about classes. *Pattern Recognition*, 26(1):155 – 165, 1993. ISSN 0031-3203. doi: [https://doi.org/10.1016/0031-3203\(93\)90097-G](https://doi.org/10.1016/0031-3203(93)90097-G). URL <http://www.sciencedirect.com/science/article/pii/003132039390097G>.
- Flach, P. and Kull, M. Precision-recall-gain curves: Pr analysis done right. In Cortes, C., Lawrence, N. D., Lee, D. D., Sugiyama, M., and Garnett, R. (eds.), *Advances in Neural Information Processing Systems 28*, pp. 838–846. Curran Associates, Inc., 2015.
- Gal, Y. and Ghahramani, Z. Dropout as a bayesian approximation: Representing model uncertainty in deep learning. In *Proceedings of the 33rd International Conference on International Conference on Machine Learning - Volume 48*, ICML’16, pp. 1050–1059. JMLR.org, 2016. URL <http://dl.acm.org/citation.cfm?id=3045390.3045502>.
- Geifman, Y. and El-Yaniv, R. Selective classification for deep neural networks. In *Proceedings of the 31st International Conference on Neural Information Processing Systems*, NIPS’17, pp. 4885–4894, Red Hook, NY, USA, 2017. Curran Associates Inc. ISBN 9781510860964.
- Goodfellow, I., Shlens, J., and Szegedy, C. Explaining and harnessing adversarial examples. *arXiv 1412.6572*, 12 2014.
- Guo, C., Pleiss, G., Sun, Y., and Weinberger, K. Q. On calibration of modern neural networks. In *Proceedings of the 34th International Conference on Machine Learning - Volume 70*, ICML’17, pp. 1321–1330. JMLR.org, 2017.
- Gupta, C. N., Palaniappan, R., Swaminathan, S., and Krishnan, S. M. Neural network classification of homomorphic segmented heart sounds. *Applied Soft Computing*, 7(1):286 – 297, 2007. ISSN 1568-4946. doi: <https://doi.org/10.1016/j.asoc.2005.06.006>. URL <http://www.sciencedirect.com/science/article/pii/S1568494605000694>.
- Haldimann, D., Blum, H., Siegwart, R., and Cadena, C. This is not what I imagined: Error detection for semantic segmentation through visual dissimilarity. *ArXiv*, abs/1909.00676, 2019.
- Hecker, S., Dai, D., and Van Gool, L. Failure prediction for autonomous driving, 05 2018.
- Hendrycks, D. and Gimpel, K. A baseline for detecting misclassified and out-of-distribution examples in neural networks. *Proceedings of International Conference on Learning Representations*, 2017.
- Hensman, J., Fusi, N., and Lawrence, N. D. Gaussian processes for big data. In *Proceedings of the Twenty-Ninth Conference on Uncertainty in Artificial Intelligence*, UAI’13, pp. 282–290, Arlington, Virginia, United States, 2013. AUAI Press. URL <http://dl.acm.org/citation.cfm?id=3023638.3023667>.
- Hensman, J., Matthews, A., and Ghahramani, Z. Scalable Variational Gaussian Process Classification. In Lebanon, G. and Vishwanathan, S. V. N. (eds.), *Proceedings of the Eighteenth International Conference on Artificial Intelligence and Statistics*, volume 38 of *Proceedings of Machine Learning Research*, pp. 351–360, San Diego, California, USA, 09–12 May 2015. PMLR. URL <http://proceedings.mlr.press/v38/hensman15.html>.
- Janai, J., Güney, F., Behl, A., and Geiger, A. Computer vision for autonomous vehicles: Problems, datasets and state-of-the-art. *ArXiv*, abs/1704.05519, 2017.
- Jiang, H., Kim, B., and Gupta, M. To trust or not to trust a classifier, 05 2018.
- Klambauer, G., Unterthiner, T., Mayr, A., and Hochreiter, S. Self-normalizing neural networks. In *Proceedings of the 31st International Conference on Neural Information Processing Systems*, NIPS’17, pp. 972–981, Red

- Hook, NY, USA, 2017. Curran Associates Inc. ISBN 9781510860964.
- Koppel, M. and Engelson, S. P. Integrating multiple classifiers by finding their areas of expertise. In *In: AAAI-96 Workshop On Integrating Multiple Learning Models*, pp. 53–58, 1996.
- Kull, M., Perello Nieto, M., Kängsepp, M., Silva Filho, T., Song, H., and Flach, P. Beyond temperature scaling: Obtaining well-calibrated multi-class probabilities with dirichlet calibration. In *Advances in Neural Information Processing Systems 32*, pp. 12316–12326. Curran Associates, Inc., 2019.
- LeCun, Y., Bengio, Y., and Hinton, G. Deep learning. *Nature*, 521:436 EP –, 05 2015. URL <https://doi.org/10.1038/nature14539>.
- Lee, K., Lee, H., Lee, K., and Shin, J. Training confidence-calibrated classifiers for detecting out-of-distribution samples. In *International Conference on Learning Representations*, 2018a. URL <https://openreview.net/forum?id=ryiAv2xAZ>.
- Lee, K., Lee, K., Lee, H., and Shin, J. A simple unified framework for detecting out-of-distribution samples and adversarial attacks. In Bengio, S., Wallach, H., Larochelle, H., Grauman, K., Cesa-Bianchi, N., and Garnett, R. (eds.), *Advances in Neural Information Processing Systems 31*, pp. 7167–7177. Curran Associates, Inc., 2018b.
- Liang, S., Li, Y., and Srikant, R. Enhancing the reliability of out-of-distribution image detection in neural networks. In *International Conference on Learning Representations*, 2018. URL <https://openreview.net/forum?id=H1VGkIXRZ>.
- Mandelbaum, A. and Weinshall, D. Distance-based confidence score for neural network classifiers. *ArXiv*, abs/1709.09844, 2017.
- Manning, C. D. and Schütze, H. *Foundations of Statistical Natural Language Processing*. MIT Press, Cambridge, MA, USA, 1999. ISBN 0262133601.
- Monteith, K. and Martinez, T. R. Using multiple measures to predict confidence in instance classification. *The 2010 International Joint Conference on Neural Networks (IJCNN)*, pp. 1–8, 2010.
- Nguyen, A., Yosinski, J., and Clune, J. Deep neural networks are easily fooled: High confidence predictions for unrecognizable images. pp. 427–436, 06 2015. doi: 10.1109/CVPR.2015.7298640.
- Niculescu-Mizil, A. and Caruana, R. Predicting good probabilities with supervised learning. In *Proceedings of the 22nd International Conference on Machine Learning, ICML '05*, pp. 625–632, New York, NY, USA, 2005. Association for Computing Machinery. ISBN 1595931805. doi: 10.1145/1102351.1102430. URL <https://doi.org/10.1145/1102351.1102430>.
- Ortega, J. Exploiting multiple existing models and learning algorithms. In *In AAAI 96 - Workshop in Induction of Multiple Learning Models*, pp. 239–266, 1995.
- Platt, J. C. Probabilistic outputs for support vector machines and comparisons to regularized likelihood methods. In *ADVANCES IN LARGE MARGIN CLASSIFIERS*, pp. 61–74. MIT Press, 1999.
- Provost, F. J., Fawcett, T., and Kohavi, R. The case against accuracy estimation for comparing induction algorithms. In *Proceedings of the Fifteenth International Conference on Machine Learning, ICML '98*, pp. 445–453, San Francisco, CA, USA, 1998. Morgan Kaufmann Publishers Inc. ISBN 1558605568.
- Qiu, X., Meyerson, E., and Miikkulainen, R. Quantifying point-prediction uncertainty in neural networks via residual estimation with an i/o kernel. In *International Conference on Learning Representations*, 2020.
- Santos-Pereira, C. M. and Pires, A. M. On optimal reject rules and roc curves. *Pattern Recogn. Lett.*, 26(7): 943–952, May 2005. ISSN 0167-8655.
- Seewald, A. K. and Fürnkranz, J. An evaluation of grading classifiers. In *Proceedings of the 4th International Conference on Advances in Intelligent Data Analysis, IDA '01*, pp. 115–124, Berlin, Heidelberg, 2001. Springer-Verlag. ISBN 3540425810.
- Selişteanu, D., Maksimenko, V. A., Kurkin, S. A., Pit-sik, E. N., Musatov, V. Y., Runnova, A. E., Efremova, T. Y., Hramov, A. E., and Pisarchik, A. N. Artificial neural network classification of motor-related eeg: An increase in classification accuracy by reducing signal complexity. *Complexity*, 2018:9385947, 2018. doi: 10.1155/2018/9385947. URL <https://doi.org/10.1155/2018/9385947>.
- Shahid, N., Rappon, T., and Berta, W. Applications of artificial neural networks in health care organizational decision-making: A scoping review. *PLOS ONE*, 14(2):1–22, 02 2019. doi: 10.1371/journal.pone.0212356. URL <https://doi.org/10.1371/journal.pone.0212356>.
- Simonyan, K. and Zisserman, A. Very deep convolutional networks for large-scale image recognition. In *International Conference on Learning Representations*, 2015.

- Snoek, J., Rippel, O., Swersky, K., Kiros, R., Satish, N., Sundaram, N., Patwary, M. M. A., Prabhat, P., and Adams, R. P. Scalable bayesian optimization using deep neural networks. In *Proceedings of the 32nd International Conference on International Conference on Machine Learning - Volume 37, ICML'15*, pp. 2171–2180. JMLR.org, 2015.
- Steinhardt, J. and Liang, P. Unsupervised risk estimation using only conditional independence structure. In *Proceedings of the 30th International Conference on Neural Information Processing Systems, NIPS'16*, pp. 3664–3672, Red Hook, NY, USA, 2016. Curran Associates Inc. ISBN 9781510838819.
- Ulapane, N., Thiyagarajan, K., and Kodagoda, S. Hyperparameter initialization for squared exponential kernel-based gaussian process regression, 03 2020.
- Wang, J., Dong, G., Sun, J., Wang, X., and Zhang, P. Adversarial sample detection for deep neural network through model mutation testing. In *2019 IEEE/ACM 41st International Conference on Software Engineering (ICSE)*, pp. 1245–1256, 2019.
- Wen, Y., Vicol, P., Ba, J., Tran, D., and Grosse, R. Flipout: Efficient pseudo-independent weight perturbations on mini-batches. In *International Conference on Learning Representations*, 2018. URL <https://openreview.net/forum?id=rJNpifWAb>.
- Williams, G. and Renals, S. Confidence measures for hybrid hmm/ann speech recognition. In *In Proceedings of EuroSpeech*, pp. 1955–1958, 1997.
- Xing, C., Arik, S., Zhang, Z., and Pfister, T. Distance-based learning from errors for confidence calibration. In *International Conference on Learning Representations*, 2020. URL <https://openreview.net/forum?id=BJeB5hVtvB>.
- Yuan, M. and Wegkamp, M. Classification methods with reject option based on convex risk minimization. *Journal of Machine Learning Research*, 11(5): 111–130, 2010. URL <http://jmlr.org/papers/v11/yuan10a.html>.
- Zadrozny, B. and Elkan, C. Obtaining calibrated probability estimates from decision trees and naive bayesian classifiers. In *Proceedings of the Eighteenth International Conference on Machine Learning, ICML '01*, pp. 609–616, San Francisco, CA, USA, 2001. Morgan Kaufmann Publishers Inc. ISBN 1558607781.
- Zadrozny, B. and Elkan, C. Transforming classifier scores into accurate multiclass probability estimates. In *Proceedings of the Eighth ACM SIGKDD International Conference on Knowledge Discovery and Data Mining*, KDD '02, pp. 694–699, New York, NY, USA, 2002. Association for Computing Machinery. ISBN 158113567X. doi: 10.1145/775047.775151. URL <https://doi.org/10.1145/775047.775151>.

A. Appendix

A.1. Experimental Setup for Section 4.1 and Section 4.2

General Information 10 independent runs are performed for each dataset. During each run, the dataset is randomly split into a training set (80%) and a testing set (20%), then a fully connected feed-forward NN classifier with 2 hidden layers, each with 64 hidden neurons, are trained on the training set. The activation function is ReLU for all the hidden layers. The maximum number of epochs for training is 1000. 20% of the training set is used as validation set, and the split is random at each independent run. An early stop is triggered if the loss on validation set has not be improved for 10 epochs. The optimizer is Adam with learning rate 0.001, $\beta_1 = 0.9$, and $\beta_2 = 0.999$. The loss function is cross entropy loss. During each independent run, the same random dataset split and trained base NN classifier is used for evaluating all algorithms. Source codes for reproducing the experimental results can be downloaded from (https://drive.google.com/file/d/1obOHiZyWI0LJFvSMwyDm_HSNOVrNhbpV/view?usp=sharing). All the experiments in this paper are running on a machine with 20 Intel(R) Xeon(R) Gold 5215 CPU @ 2.50GHz, 128GB memory, and a GTX 2080.

Dataset Description In total, 125 UCI datasets are used in the experiments, among which 121 are from Klambauer et al. (2017), and 4 are recent datasets released in Dua & Graff (2017). All features in all datasets are normalized to have mean 0 and standard deviation 1. Full details regarding the number of samples N, number of features M, and number of classes K for each dataset are shown in Table 5.

Parametric Setup for Algorithms

- RED: SVGP (Hensman et al., 2013; 2015) is used as an approximator to original GP. The number of inducing points is 50. RBF kernel is used for both input and multi-output kernel. Automatic Relevance Determination (ARD) feature is turned on. The signal variances and length scales of all the kernels plus the noise variance are the trainable hyperparameters. The optimizer is L-BFGS-B with default parameters as in Scipy.optimize documentation (<https://docs.scipy.org/doc/scipy/reference/optimize.minimize-lbfgsb.html>), and the maximum number of iterations is set as 1000. The optimization process runs until the L-BFGS-B optimizer decides to stop. To overcome

the sensitivity of GP optimization to initialization of the hyperparameters (Ulapane et al., 2020), 20 random initialization of the hyperparameters are tried for each independent run. For each random initialization, the signal variances are generated from a uniform distribution within interval $[0, 1]$, and the lengthscales are generated from a uniform distribution within interval $[0, 10]$. For 10 initializations, the hyperparameters of input kernel are first optimized while the multi-output kernel is temporarily turned off, then after the optimizer stops, the multi-output kernel is turned on, and both the two kernels are optimized simultaneously. For the other 10 initializations, both kernels are optimized simultaneously from the start. The average performance of the 3 best optimized model in terms of corresponding metrics are used as the final performance of RED on each independent run. During our preliminary investigation, several statistic metrics on training set is effective in picking the true best-performing model out of these 20 trials, e.g., the gap between average estimated detection scores of correctly classified training samples and incorrectly classified training samples, the scale of optimized noise variance of SVGP model, the ratio between sum of signal variances and noise variance after optimization, etc. Since improving initialization and optimization of GP hyperparameters is out of the scope of this work, we simply use average performance of the best 3 models (top 15%) in comparison.

- MCP baseline: The maximum class probability of softmax outputs of the base NN classifier is used as the detection score of MCP baseline. The setup of the base NN classifier is provided above.
- Trust Score: $k=10$, $\alpha=0$, without filtering. This is the same as the default setup in <https://github.com/google/TrustScore>.
- ConfidNet: During training, the input to ConfidNet is the raw feature, and the target is the class probability of the ground-truth class returned by base NN classifier. The architecture of ConfidNet is a fully connected feed-forward NN regressor with 2 hidden layers, each with 64 hidden neurons. The activation function is ReLU for all the hidden layers. The maximum number of epochs for training is 1000. An early stop is triggered if the loss on validation data has not be improved for 10 epochs. The optimizer is RMSprop with learning rate 0.001, and the loss function is mean squared error (MSE).
- Introspection-Net: During training, the input to Introspection-Net is the logit outputs of base NN classifier, and the target is 1 for correctly classified sample, and 0 for incorrectly classified sample. The architecture of ConfidNet is a fully connected feed-forward NN regressor with 2 hidden layers, each with 64 hidden neurons. The activation function is ReLU for all the hidden layers. The maximum number of epochs for training is 1000. An early stop is triggered if the loss on validation data has not be improved for 10 epochs. The optimizer is RMSprop with learning rate 0.001, and the loss function is mean squared error (MSE).
- Entropy: The entropy of softmax outputs of the base NN classifier is used as the detection score of Entropy. The setup of the base NN classifier is provided above.
- DNGO: A Bayesian linear regression layer similar to that of Snoek et al. (2015) is added after the logits layer of the original NN classifier to predict whether an original prediction is correct or not (1 for correct and 0 for incorrect). Default parametric setup, as in <https://github.com/automl/pybnn/blob/master/pybnn/dngo.py>, is used.
- SVGP: The original SVGP without output kernel is used to predict directly whether a prediction made by the base NN classifier is correct or not (1 for correct and 0 for incorrect). All other parameters are identical to those in RED.
- BNN MCP: The standard dense layers in the base NN classifier described in RED setup above is replaced with Flipout layers (Wen et al., 2018). All other parameters are identical with those in RED. The maximum class probability averaging over 100 test-time samplings is used as the detection score for error detection.
- BNN Entropy: The same setup as with BNN MCP, except now the entropy of softmax outputs averaging over 100 test-time samplings is used as the detection score for error detection.
- MC-Dropout MCP: A dropout layer with dropout rate of 0.5 is added after each dense layer of the base NN classifier described in the RED setup. All other parameters are identical with those in RED. The maximum class probability averaging over 100 test-time Monte-Carlo samplings is used as the detection score for error detection.
- MC-Dropout Entropy: The same setup as with MC-Dropout MCP, except now the entropy of softmax outputs is averaged over 100 test-time Monte-Carlo samplings and used as detection score for error detection.

A.2. Experimental Setup for Section 4.3

Setup of VGG16 Training The standard VGG16 architecture (Simonyan & Zisserman, 2015) is

used. The training pipeline is based on the default setup described in <https://github.com/geifmany/cifar-vgg/blob/master/cifar10vgg.py>. For the CIFAR-10 dataset, 40,000 samples are used as the training set, 10,000 as the validation set, and 10,000 as the testing set.

Parametric Setup for Algorithms All algorithms use the logit outputs of the trained VGG16 model as input features. The maximum class probability of softmax outputs of the trained VGG16 model is used as the detection score of MCP baseline. The parameters for RED, Trust Score, Entropy, DNGO and SVGP are identical to those in the UCI experiments. For ConfidNet and Introspection-Net, all parameters are the same as in the UCI experiments, except for that the number of hidden neurons for all hidden layers is increased to 128.

A.3. Detailed Results for Section 4.1 and Section 4.2

This subsection shows all the detailed results for experiments performed in Section 4.1 and Section 4.2. The results are averaged over 10 independent runs in terms of AP-Error, AP-Success, AUPR-Error, AUPR-Success, and AUROC. Detailed results for Section 4.1 are shown in Table 5, Table 6, Table 7, Table 8, and Table 9. Detailed results for Section 4.2 are shown in Table 10, Table 11, Table 12, Table 13, and Table 14. Each table is corresponding to one performance metric. The column "N", "M", and "K" denotes the number of samples, number of features, and number of classes for corresponding datasets. To save space, "MCP", "Intro-Net", "MC-D" stands for "MCP Baseline", "Introspection-Net", and "MC-Dropout", respectively. For datasets that the original NN classifier achieves 100% accuracy, the entries are marked as "NA". For dataset splits that the number of samples in one particular class is too small for Trust Score to calculate neighborhood distance, the entries are marked as "NA".

Detecting Misclassification Errors in Neural Networks with a Gaussian Process Model

Table 5: Comparison between RED and Counterparts Using AP-Error

Dataset	N	M	K	RED	MCP	Trust Score	ConfidNet	Intro-Net	Entropy	DNGO	SVGP
abalone	4177	8	3	0.546	0.539	0.480	0.518	0.528	0.529	0.496	0.482
acute-inflammation	120	6	2	NA	NA	NA	NA	NA	NA	NA	NA
acute-nephritis	120	6	2	NA	NA	NA	NA	NA	NA	NA	NA
adult	48842	14	2	0.419	0.411	0.328	0.391	0.412	0.411	0.338	0.358
annealing	898	31	5	0.558	0.392	0.453	0.350	0.399	0.368	0.314	0.324
arrhythmia	452	262	13	0.583	0.580	0.618	0.409	0.413	0.560	0.426	0.475
audiology-std	196	59	18	0.779	0.721	NA	0.428	0.518	0.731	0.590	0.556
balance-scale	625	4	3	0.888	0.816	0.540	0.046	0.155	0.730	0.319	0.128
balloons	16	4	2	0.840	0.806	0.704	0.694	0.806	0.806	0.615	0.583
bank	4521	16	2	0.397	0.393	0.390	0.372	0.339	0.393	0.108	0.383
bioconcentration	779	9	3	0.493	0.470	0.510	0.426	0.461	0.440	0.408	0.385
blood	748	4	2	0.390	0.389	0.272	0.382	0.372	0.389	0.319	0.362
breast-cancer	286	9	2	0.532	0.503	0.381	0.467	0.431	0.503	0.441	0.471
breast-cancer-wisc	699	9	2	0.423	0.393	0.405	0.313	0.245	0.393	0.175	0.152
breast-cancer-wisc-diag	569	30	2	0.626	0.599	0.500	0.089	0.374	0.601	0.089	0.119
breast-cancer-wisc-prog	198	33	2	0.408	0.403	0.296	0.343	0.373	0.403	0.288	0.266
breast-tissue	106	9	6	0.813	0.743	0.800	0.696	0.601	0.749	0.744	0.722
car	1728	6	4	0.571	0.462	0.256	0.140	0.053	0.457	0.117	0.098
cardiotocography-10clases	2126	21	10	0.513	0.492	0.400	0.310	0.302	0.472	0.303	0.290
cardiotocography-3clases	2126	21	3	0.439	0.386	0.393	0.273	0.282	0.382	0.125	0.284
chess-krvk	28056	6	18	0.550	0.523	0.715	0.486	0.449	0.515	0.386	0.405
chess-krvkv	3196	36	2	0.347	0.339	0.163	0.037	0.087	0.339	0.038	0.054
climate	540	20	2	0.456	0.428	0.276	0.093	0.394	0.428	0.095	0.132
congressional-voting	435	16	2	0.468	0.465	0.429	0.474	0.459	0.464	0.478	0.470
conn-bench-sonar-mines-rocks	208	60	2	0.545	0.531	0.697	0.296	0.343	0.531	0.391	0.304
conn-bench-vowel-deterding	990	11	11	0.689	0.523	0.875	0.148	0.170	0.493	0.271	0.200
connect-4	67557	42	2	0.406	0.390	0.326	0.259	0.395	0.390	0.321	0.155
contrac	1473	9	3	0.596	0.590	0.529	0.552	0.584	0.577	0.573	0.548
credit-approval	690	15	2	0.365	0.359	0.336	0.264	0.331	0.359	0.302	0.336
cylinder-bands	512	35	2	0.494	0.482	0.506	0.345	0.422	0.482	0.383	0.304
dermatology	366	34	6	0.690	0.648	0.605	0.072	0.253	0.686	0.327	0.130
echocardiogram	131	10	2	0.510	0.413	0.325	0.353	0.407	0.413	0.306	0.375
ecoli	336	7	8	0.433	0.421	0.472	0.283	0.284	0.374	0.278	0.286
energy-y1	768	8	3	0.472	0.380	0.289	0.195	0.187	0.364	0.144	0.244
energy-y2	768	8	3	0.498	0.434	0.498	0.322	0.278	0.421	0.302	0.328
fertility	100	9	2	0.267	0.238	0.239	0.193	0.217	0.238	0.169	0.160
flags	194	28	8	0.767	0.717	0.784	0.666	0.664	0.712	0.649	0.659
glass	214	9	6	0.583	0.525	0.657	0.507	0.412	0.489	0.498	0.414
haberman-survival	306	3	2	0.452	0.446	0.386	0.412	0.425	0.446	0.360	0.499
hayes-roth	160	3	3	0.688	0.576	0.728	0.603	0.572	0.576	0.657	0.536
heart-cleveland	303	13	5	0.759	0.748	0.707	0.689	0.705	0.732	0.627	0.730
heart-hungarian	294	12	2	0.436	0.418	0.442	0.261	0.397	0.418	0.356	0.351
heart-switzerland	123	12	5	0.735	0.692	0.726	0.697	0.662	0.700	0.705	0.649
heart-va	200	12	5	0.757	0.732	0.676	0.678	0.732	0.746	0.677	0.639
hepatitis	155	19	2	0.542	0.441	0.495	0.423	0.330	0.441	0.408	0.369
hill-valley	1212	100	2	0.657	0.546	0.478	0.508	0.594	0.546	0.554	0.546
horse-colic	368	25	2	0.444	0.431	0.426	0.263	0.394	0.431	0.304	0.247
ilpd-indian-liver	583	9	2	0.470	0.459	0.427	0.434	0.443	0.459	0.375	0.445
image-segmentation	2310	18	7	0.539	0.455	0.471	0.251	0.214	0.430	0.218	0.139
ionosphere	351	33	2	0.543	0.493	0.335	0.158	0.405	0.493	0.300	0.171
iris	150	4	3	0.686	0.633	0.747	0.154	0.202	0.605	0.360	0.227
led-display	1000	7	10	0.572	0.571	0.301	0.553	0.512	0.547	0.508	0.470
lenses	24	4	3	0.875	0.900	0.786	0.665	0.790	0.900	0.622	0.587
letter	20000	16	26	0.495	0.461	0.785	0.245	0.081	0.465	0.109	0.164
libras	360	90	15	0.602	0.512	0.657	0.307	0.301	0.479	0.498	0.279
low-res-spect	531	100	9	0.552	0.515	0.454	0.304	0.305	0.504	0.297	0.343
lung-cancer	32	56	3	0.887	0.819	0.695	0.690	0.841	0.859	0.641	0.582
lymphography	148	18	4	0.660	0.546	0.619	0.278	0.386	0.545	0.353	0.363
magic	19020	10	2	0.366	0.355	0.294	0.309	0.350	0.355	0.240	0.233
mammographic	961	5	2	0.471	0.468	0.288	0.414	0.454	0.468	0.386	0.402
messidor	1151	19	2	0.465	0.449	0.359	0.364	0.426	0.449	0.411	0.350
miniboone	130064	50	2	0.380	0.361	0.190	0.299	0.371	0.361	0.251	0.162
molec-biol-promoter	106	57	2	0.550	0.541	0.786	0.330	0.505	0.541	0.432	0.437
molec-biol-splice	3190	60	3	0.461	0.455	0.375	0.193	0.208	0.464	0.396	0.174
monks-1	556	6	2	0.618	0.444	0.167	0.242	0.343	0.444	0.110	0.222
monks-2	601	6	2	0.524	0.466	0.611	0.417	0.426	0.466	0.389	0.387
monks-3	554	6	2	0.648	0.561	0.369	0.319	0.453	0.561	0.395	0.175
mushroom	8124	21	2	NA	NA	NA	NA	NA	NA	NA	NA
musk-1	476	166	2	0.518	0.508	0.501	0.101	0.354	0.508	0.295	0.103
musk-2	6598	166	2	0.409	0.372	0.083	0.009	0.077	0.372	0.006	0.007
nursery	12960	8	5	0.586	0.448	0.074	0.035	0.127	0.447	0.135	0.173
oocytes_merluccius_nucleus_4d	1022	41	2	0.442	0.401	0.277	0.296	0.383	0.401	0.385	0.330
oocytes_merluccius_states_2f	1022	25	3	0.505	0.488	0.413	0.256	0.358	0.477	0.214	0.262
oocytes_trisopterus_nucleus_2f	912	25	2	0.481	0.451	0.342	0.275	0.460	0.451	0.354	0.300
oocytes_trisopterus_states_5b	912	32	3	0.445	0.423	0.346	0.155	0.291	0.441	0.316	0.114

Continued on next page.

Detecting Misclassification Errors in Neural Networks with a Gaussian Process Model

Dataset	N	M	K	RED	MCP	Trust Score	ConfidNet	Intro-Net	Entropy	DNGO	SVGP
optical	5620	62	10	0.452	0.429	0.582	0.048	0.036	0.422	0.079	0.068
ozone	2536	72	2	0.308	0.293	0.270	0.207	0.146	0.293	0.032	0.025
page-blocks	5473	10	5	0.450	0.386	0.399	0.330	0.275	0.371	0.254	0.186
parkinsons	195	22	2	0.562	0.516	0.541	0.155	0.239	0.516	0.276	0.316
pendigits	10992	16	10	0.491	0.362	0.684	0.178	0.132	0.363	0.104	0.059
phishing	1353	9	3	0.453	0.433	0.369	0.347	0.371	0.412	0.338	0.334
pima	768	8	2	0.501	0.492	0.422	0.412	0.486	0.492	0.426	0.336
pittsburg-bridges-MATERIAL	106	7	3	0.600	0.501	0.485	0.360	0.511	0.506	0.336	0.392
pittsburg-bridges-REL-L	103	7	3	0.593	0.536	0.654	0.522	0.549	0.529	0.501	0.498
pittsburg-bridges-SPAN	92	7	3	0.582	0.550	0.543	0.367	0.507	0.563	0.472	0.449
pittsburg-bridges-T-OR-D	102	7	2	0.472	0.397	0.456	0.391	0.506	0.397	0.375	0.352
pittsburg-bridges-TYPE	105	7	6	0.809	0.736	0.758	0.684	0.662	0.692	0.702	0.737
planning	182	12	2	0.366	0.364	0.387	0.348	0.331	0.364	0.312	0.259
plant-margin	1600	64	100	0.586	0.572	0.696	0.331	0.266	0.569	0.305	0.183
plant-shape	1600	64	100	0.693	0.666	0.759	0.524	0.477	0.643	0.517	0.477
plant-texture	1599	64	100	0.607	0.596	0.708	0.308	0.291	0.610	0.282	0.221
post-operative	90	8	3	0.428	0.416	0.289	0.377	0.413	0.374	0.441	0.418
primary-tumor	330	17	15	0.794	0.783	0.693	0.725	0.721	0.779	0.683	0.715
ringnorm	7400	20	2	0.348	0.344	0.275	0.042	0.116	0.344	0.112	0.027
seeds	210	7	3	0.583	0.514	0.526	0.344	0.333	0.475	0.397	0.345
semeion	1593	256	10	0.541	0.527	0.704	0.092	0.237	0.564	0.180	0.142
soybean	683	35	18	0.573	0.516	0.448	0.317	0.191	0.505	0.234	0.319
spambase	4601	57	2	0.316	0.292	0.299	0.179	0.238	0.292	0.203	0.139
spect	265	22	2	0.520	0.506	0.384	0.443	0.471	0.506	0.419	0.434
spectf	267	44	2	0.478	0.427	0.429	0.251	0.428	0.427	0.258	0.346
statlog-australian-credit	690	14	2	0.473	0.455	0.418	0.417	0.416	0.455	0.407	0.430
statlog-german-credit	1000	24	2	0.423	0.422	0.383	0.329	0.389	0.422	0.354	0.254
statlog-heart	270	13	2	0.471	0.438	0.388	0.322	0.462	0.438	0.350	0.285
statlog-image	2310	18	7	0.561	0.464	0.484	0.240	0.114	0.473	0.274	0.183
statlog-landsat	6435	36	6	0.430	0.398	0.554	0.322	0.312	0.409	0.288	0.255
statlog-shuttle	58000	9	7	0.551	0.318	0.547	0.233	0.157	0.310	0.139	0.247
statlog-vehicle	846	18	4	0.542	0.526	0.319	0.392	0.361	0.536	0.346	0.364
steel-plates	1941	27	7	0.529	0.517	0.533	0.452	0.437	0.514	0.437	0.404
synthetic-control	600	60	6	0.647	0.541	0.462	0.052	0.117	0.498	0.199	0.031
teaching	151	5	3	0.646	0.604	0.540	0.632	0.593	0.612	0.676	0.569
thyroid	7200	21	3	0.442	0.413	0.160	0.126	0.190	0.409	0.015	0.114
tic-tac-toe	958	9	2	0.633	0.538	1.000	0.160	0.513	0.538	0.385	0.480
titanic	2201	3	2	0.314	0.313	0.202	0.310	0.315	0.313	0.227	0.321
trains	10	29	2	0.778	0.750	0.917	0.833	0.750	0.750	0.625	0.750
twonorm	7400	20	2	0.371	0.357	0.404	0.160	0.290	0.357	0.176	0.037
vertebral-column-2clases	310	6	2	0.501	0.490	0.346	0.378	0.432	0.490	0.389	0.273
vertebral-column-3clases	310	6	3	0.542	0.518	0.308	0.489	0.396	0.529	0.439	0.307
wall-following	5456	24	4	0.418	0.378	0.304	0.208	0.248	0.370	0.261	0.139
waveform	5000	21	3	0.465	0.423	0.331	0.357	0.394	0.423	0.200	0.162
waveform-noise	5000	40	3	0.428	0.398	0.322	0.230	0.326	0.397	0.215	0.167
wine	178	13	3	0.894	0.742	0.661	0.101	0.458	0.825	0.613	0.284
wine-quality-red	1599	11	6	0.534	0.522	0.540	0.494	0.491	0.496	0.523	0.453
wine-quality-white	4898	11	7	0.541	0.529	0.626	0.534	0.523	0.516	0.524	0.480
yeast	1484	8	10	0.570	0.563	0.510	0.506	0.498	0.548	0.410	0.912
zoo	101	16	7	0.910	0.804	0.793	0.297	0.546	0.893	0.443	0.694

Continued from previous page.

Table 6: Comparison between RED and Counterparts Using AP-Success

Dataset	N	M	K	RED	MCP	Trust Score	ConfidNet	Intro-Net	Entropy	DNGO	SVGP
abalone	4177	8	3	0.853	0.850	0.821	0.845	0.844	0.849	0.814	0.840
acute-inflammation	120	6	2	NA	NA	NA	NA	NA	NA	NA	NA
acute-nephritis	120	6	2	NA	NA	NA	NA	NA	NA	NA	NA
adult	48842	14	2	0.968	0.967	0.944	0.964	0.961	0.967	0.927	0.961
annealing	898	31	5	0.975	0.899	0.943	0.909	0.916	0.902	0.898	0.913
arrhythmia	452	262	13	0.817	0.810	0.809	0.654	0.668	0.803	0.673	0.778
audiology-std	196	59	18	0.946	0.926	NA	0.625	0.740	0.927	0.756	0.782
balance-scale	625	4	3	0.999	0.999	0.997	0.972	0.983	0.999	0.985	0.976
balloons	16	4	2	0.843	0.806	0.806	0.769	0.806	0.806	0.625	0.667
bank	4521	16	2	0.977	0.980	0.976	0.968	0.937	0.980	0.892	0.979
bioconcentration	779	9	3	0.746	0.728	0.782	0.717	0.726	0.721	0.693	0.698
blood	748	4	2	0.892	0.892	0.873	0.902	0.883	0.892	0.869	0.900
breast-cancer	286	9	2	0.820	0.820	0.765	0.796	0.775	0.820	0.767	0.785
breast-cancer-wisc	699	9	2	0.998	0.997	0.998	0.994	0.985	0.997	0.987	0.986
breast-cancer-wisc-diag	569	30	2	0.996	0.996	0.997	0.970	0.981	0.998	0.973	0.981
breast-cancer-wisc-prog	198	33	2	0.856	0.860	0.797	0.824	0.835	0.860	0.787	0.795
breast-tissue	106	9	6	0.909	0.878	0.898	0.863	0.767	0.872	0.800	0.849
car	1728	6	4	0.999	0.999	0.999	0.992	0.988	0.999	0.984	0.990
cardiotocography-10clases	2126	21	10	0.959	0.959	0.927	0.890	0.872	0.958	0.885	0.901

Continued on next page.

Detecting Misclassification Errors in Neural Networks with a Gaussian Process Model

Dataset	N	M	K	RED	MCP	Trust Score	ConfidNet	Intro-Net	Entropy	DNGO	SVGP
cardiotocography-3clases	2126	21	3	0.990	0.991	0.988	0.972	0.964	0.991	0.935	0.979
chess-krvk	28056	6	18	0.900	0.890	0.934	0.867	0.838	0.889	0.782	0.801
chess-krvkp	3196	36	2	1.000	1.000	0.995	0.990	0.994	1.000	0.993	0.996
climate	540	20	2	0.991	0.989	0.976	0.938	0.976	0.987	0.945	0.950
congressional-voting	435	16	2	0.693	0.690	0.672	0.692	0.684	0.689	0.691	0.689
conn-bench-sonar-mines-rocks	208	60	2	0.962	0.963	0.980	0.815	0.901	0.963	0.874	0.897
conn-bench-vowel-deterding	990	11	11	1.000	1.000	1.000	0.980	0.984	1.000	0.989	0.989
connect-4	67557	42	2	0.969	0.969	0.938	0.942	0.958	0.969	0.927	0.868
contrac	1473	9	3	0.717	0.714	0.581	0.682	0.675	0.705	0.658	0.669
credit-approval	690	15	2	0.943	0.941	0.916	0.909	0.936	0.941	0.896	0.928
cylinder-bands	512	35	2	0.865	0.862	0.872	0.789	0.809	0.862	0.767	0.758
dermatology	366	34	6	0.999	0.999	0.997	0.975	0.981	0.999	0.977	0.951
echocardiogram	131	10	2	0.944	0.936	0.925	0.916	0.924	0.936	0.888	0.929
ecoli	336	7	8	0.959	0.956	0.969	0.911	0.879	0.954	0.886	0.919
energy-y1	768	8	3	0.992	0.994	0.992	0.975	0.974	0.994	0.959	0.983
energy-y2	768	8	3	0.986	0.986	0.985	0.962	0.946	0.986	0.963	0.978
fertility	100	9	2	0.953	0.928	0.948	0.920	0.929	0.928	0.903	0.939
flags	194	28	8	0.739	0.716	0.817	0.573	0.617	0.720	0.580	0.599
glass	214	9	6	0.854	0.811	0.915	0.779	0.738	0.810	0.741	0.783
haberman-survival	306	3	2	0.850	0.849	0.854	0.821	0.835	0.849	0.818	0.835
hayes-roth	160	3	3	0.931	0.881	0.959	0.887	0.864	0.887	0.881	0.837
heart-cleveland	303	13	5	0.856	0.859	0.836	0.800	0.822	0.861	0.696	0.838
heart-hungarian	294	12	2	0.925	0.908	0.927	0.847	0.915	0.908	0.844	0.869
heart-switzerland	123	12	5	0.500	0.480	0.478	0.451	0.452	0.490	0.471	0.446
heart-va	200	12	5	0.526	0.499	0.462	0.439	0.504	0.511	0.417	0.392
hepatitis	155	19	2	0.965	0.965	0.975	0.930	0.896	0.965	0.897	0.915
hill-valley	1212	100	2	0.763	0.704	0.559	0.653	0.741	0.704	0.698	0.693
horse-colic	368	25	2	0.927	0.918	0.920	0.833	0.913	0.918	0.836	0.871
ilpd-indian-liver	583	9	2	0.878	0.874	0.814	0.860	0.863	0.874	0.800	0.871
image-segmentation	2310	18	7	0.997	0.997	0.998	0.983	0.984	0.997	0.981	0.985
ionosphere	351	33	2	0.990	0.988	0.976	0.900	0.973	0.988	0.931	0.934
iris	150	4	3	0.992	0.991	0.997	0.938	0.917	0.991	0.950	0.955
led-display	1000	7	10	0.883	0.883	0.759	0.874	0.850	0.880	0.835	0.847
lenses	24	4	3	0.982	0.960	0.944	0.871	0.883	0.960	0.859	0.844
letter	20000	16	26	0.995	0.996	0.999	0.980	0.947	0.996	0.963	0.982
libras	360	90	15	0.956	0.943	0.956	0.808	0.807	0.941	0.863	0.850
low-res-spect	531	100	9	0.977	0.968	0.953	0.908	0.892	0.968	0.902	0.950
lung-cancer	32	56	3	0.771	0.734	0.650	0.547	0.743	0.739	0.496	0.459
lymphography	148	18	4	0.941	0.925	0.958	0.809	0.861	0.924	0.865	0.826
magic	19020	10	2	0.966	0.966	0.954	0.961	0.959	0.966	0.907	0.946
mammographic	961	5	2	0.922	0.919	0.882	0.910	0.911	0.919	0.882	0.926
messidor	1151	19	2	0.863	0.861	0.764	0.806	0.830	0.861	0.808	0.806
miniboone	130064	50	2	0.992	0.992	0.983	0.988	0.986	0.992	0.972	0.981
molec-biol-promoter	106	57	2	0.892	0.888	0.953	0.724	0.880	0.888	0.784	0.822
molec-biol-splice	3190	60	3	0.953	0.953	0.926	0.833	0.846	0.952	0.901	0.838
monks-1	556	6	2	0.998	0.997	0.984	0.988	0.989	0.997	0.981	0.995
monks-2	601	6	2	0.885	0.857	0.918	0.809	0.810	0.857	0.761	0.808
monks-3	554	6	2	0.999	0.999	0.993	0.981	0.993	0.999	0.981	0.991
mushroom	8124	21	2	NA	NA	NA	NA	NA	NA	NA	NA
musk-1	476	166	2	0.984	0.983	0.986	0.912	0.957	0.983	0.942	0.934
musk-2	6598	166	2	1.000	1.000	0.998	0.995	0.995	1.000	0.994	0.994
nursery	12960	8	5	1.000	1.000	1.000	0.999	0.999	1.000	0.999	1.000
oocytes_merluccius_nucleus_4d	1022	41	2	0.939	0.930	0.881	0.892	0.904	0.930	0.890	0.907
oocytes_merluccius_states_2f	1022	25	3	0.991	0.991	0.991	0.967	0.970	0.991	0.950	0.975
oocytes_trisopterus_nucleus_2f	912	25	2	0.940	0.931	0.908	0.872	0.923	0.931	0.873	0.876
oocytes_trisopterus_states_5b	912	32	3	0.991	0.990	0.985	0.952	0.967	0.990	0.955	0.945
optical	5620	62	10	0.999	0.999	0.999	0.981	0.981	0.999	0.982	0.992
ozone	2536	72	2	0.994	0.996	0.993	0.988	0.966	0.996	0.968	0.951
page-blocks	5473	10	5	0.998	0.997	0.993	0.993	0.989	0.997	0.989	0.994
parkinsons	195	22	2	0.994	0.992	0.995	0.939	0.944	0.992	0.962	0.964
pendigits	10992	16	10	0.999	0.999	1.000	0.992	0.992	0.999	0.994	0.993
phishing	1353	9	3	0.975	0.973	0.958	0.959	0.946	0.972	0.929	0.952
pima	768	8	2	0.898	0.894	0.875	0.848	0.873	0.894	0.857	0.870
pittsburg-bridges-MATERIAL	106	7	3	0.976	0.969	0.953	0.921	0.933	0.969	0.892	0.939
pittsburg-bridges-REL-L	103	7	3	0.790	0.780	0.845	0.766	0.744	0.783	0.735	0.773
pittsburg-bridges-SPAN	92	7	3	0.851	0.808	0.785	0.678	0.756	0.805	0.782	0.716
pittsburg-bridges-T-OR-D	102	7	2	0.957	0.943	0.924	0.926	0.946	0.943	0.932	0.920
pittsburg-bridges-TYPE	105	7	6	0.818	0.692	0.747	0.651	0.635	0.664	0.737	0.766
planning	182	12	2	0.729	0.722	0.737	0.730	0.728	0.722	0.734	0.692
plant-margin	1600	64	100	0.951	0.950	0.966	0.828	0.817	0.950	0.816	0.731
plant-shape	1600	64	100	0.861	0.849	0.880	0.718	0.671	0.838	0.697	0.673
plant-texture	1599	64	100	0.953	0.950	0.958	0.809	0.804	0.950	0.789	0.791
post-operative	90	8	3	0.683	0.673	0.739	0.684	0.685	0.670	0.727	0.687
primary-tumor	330	17	15	0.762	0.752	0.654	0.640	0.633	0.750	0.546	0.642
ringnorm	7400	20	2	0.999	0.999	0.989	0.982	0.977	0.999	0.981	0.976
seeds	210	7	3	0.988	0.986	0.992	0.964	0.961	0.985	0.935	0.947
semeion	1593	256	10	0.994	0.994	0.996	0.927	0.950	0.994	0.943	0.963

Continued on next page.

Detecting Misclassification Errors in Neural Networks with a Gaussian Process Model

Dataset	N	M	K	RED	MCP	Trust Score	ConfidNet	Intro-Net	Entropy	DNGO	SVGP
soybean	683	35	18	0.996	0.995	0.993	0.970	0.942	0.995	0.944	0.974
spambase	4601	57	2	0.989	0.988	0.984	0.965	0.966	0.988	0.962	0.974
spect	265	22	2	0.811	0.802	0.767	0.731	0.788	0.801	0.686	0.733
spectf	267	44	2	0.955	0.951	0.942	0.913	0.919	0.953	0.879	0.949
statlog-australian-credit	690	14	2	0.701	0.692	0.656	0.668	0.678	0.692	0.629	0.662
statlog-german-credit	1000	24	2	0.890	0.891	0.873	0.837	0.850	0.891	0.821	0.782
statlog-heart	270	13	2	0.940	0.935	0.906	0.882	0.917	0.935	0.853	0.863
statlog-image	2310	18	7	0.998	0.998	0.998	0.986	0.980	0.998	0.984	0.990
statlog-landsat	6435	36	6	0.986	0.987	0.991	0.964	0.959	0.987	0.953	0.971
statlog-shuttle	58000	9	7	1.000	1.000	1.000	0.998	0.998	0.999	0.999	0.999
statlog-vehicle	846	18	4	0.966	0.967	0.927	0.929	0.913	0.968	0.870	0.922
steel-plates	1941	27	7	0.919	0.917	0.928	0.882	0.850	0.916	0.827	0.870
synthetic-control	600	60	6	1.000	1.000	0.999	0.986	0.988	1.000	0.988	0.986
teaching	151	5	3	0.686	0.648	0.598	0.657	0.640	0.634	0.682	0.632
thyroid	7200	21	3	0.999	0.999	0.996	0.992	0.984	0.999	0.985	0.996
tic-tac-toe	958	9	2	1.000	0.999	1.000	0.999	0.998	0.999	0.994	0.999
titanic	2201	3	2	0.877	0.876	0.805	0.874	0.873	0.876	0.821	0.877
trains	10	29	2	0.778	0.750	0.917	0.833	0.750	0.750	0.625	0.750
twonorm	7400	20	2	0.998	0.999	0.998	0.991	0.991	0.999	0.981	0.973
vertebral-column-2clases	310	6	2	0.977	0.977	0.953	0.952	0.942	0.977	0.917	0.937
vertebral-column-3clases	310	6	3	0.978	0.977	0.943	0.959	0.933	0.978	0.912	0.953
wall-following	5456	24	4	0.980	0.980	0.972	0.928	0.949	0.980	0.945	0.933
waveform	5000	21	3	0.968	0.966	0.947	0.947	0.941	0.966	0.866	0.848
waveform-noise	5000	40	3	0.962	0.962	0.935	0.881	0.900	0.962	0.872	0.844
wine	178	13	3	0.999	0.999	0.998	0.948	0.990	0.999	0.969	0.978
wine-quality-red	1599	11	6	0.735	0.727	0.751	0.705	0.696	0.719	0.695	0.697
wine-quality-white	4898	11	7	0.673	0.663	0.745	0.650	0.655	0.656	0.652	0.611
yeast	1484	8	10	0.756	0.751	0.706	0.718	0.692	0.745	0.601	0.579
zoo	101	16	7	0.999	0.998	0.997	0.928	0.963	0.999	0.963	0.950

Continued from previous page.

Table 7: Comparison between RED and Counterparts Using AUPR-Error

Dataset	N	M	K	RED	MCP	Trust Score	ConfidNet	Intro-Net	Entropy	DNGO	SVGP
abalone	4177	8	3	0.543	0.537	0.478	0.516	0.526	0.527	0.498	0.480
acute-inflammation	120	6	2	NA	NA	NA	NA	NA	NA	NA	NA
acute-nephritis	120	6	2	NA	NA	NA	NA	NA	NA	NA	NA
adult	48842	14	2	0.419	0.410	0.328	0.390	0.412	0.410	0.372	0.357
annealing	898	31	5	0.547	0.375	0.440	0.331	0.385	0.350	0.347	0.352
arrhythmia	452	262	13	0.573	0.570	0.606	0.396	0.399	0.547	0.412	0.465
audiology-std	196	59	18	0.766	0.704	NA	0.401	0.494	0.712	0.564	0.532
balance-scale	625	4	3	0.877	0.794	0.501	0.030	0.124	0.685	0.396	0.085
balloons	16	4	2	0.785	0.736	0.796	0.569	0.736	0.736	0.479	0.458
bank	4521	16	2	0.391	0.387	0.385	0.367	0.333	0.387	0.554	0.377
bioconcentration	779	9	3	0.485	0.461	0.501	0.418	0.453	0.431	0.398	0.376
blood	748	4	2	0.377	0.375	0.312	0.367	0.357	0.377	0.345	0.348
breast-cancer	286	9	2	0.518	0.483	0.354	0.447	0.405	0.483	0.421	0.452
breast-cancer-wisc	699	9	2	0.374	0.341	0.347	0.253	0.184	0.341	0.367	0.121
breast-cancer-wisc-diag	569	30	2	0.594	0.561	0.438	0.070	0.348	0.562	0.170	0.100
breast-cancer-wisc-prog	198	33	2	0.374	0.369	0.254	0.310	0.344	0.369	0.259	0.236
breast-tissue	106	9	6	0.795	0.717	0.771	0.660	0.556	0.722	0.717	0.690
car	1728	6	4	0.537	0.419	0.236	0.111	0.041	0.413	0.317	0.081
cardiotocography-10clases	2126	21	10	0.507	0.486	0.394	0.301	0.295	0.465	0.297	0.284
cardiotocography-3clases	2126	21	3	0.429	0.372	0.377	0.259	0.268	0.369	0.493	0.272
chess-krvk	28056	6	18	0.550	0.523	0.715	0.485	0.448	0.514	0.386	0.404
chess-krvkp	3196	36	2	0.308	0.299	0.141	0.024	0.067	0.299	0.245	0.036
climate	540	20	2	0.421	0.395	0.239	0.081	0.362	0.395	0.296	0.110
congressional-voting	435	16	2	0.503	0.503	0.659	0.505	0.543	0.488	0.503	0.511
conn-bench-sonar-mines-rocks	208	60	2	0.507	0.487	0.666	0.260	0.305	0.487	0.352	0.264
conn-bench-vowel-deterding	990	11	11	0.636	0.455	0.865	0.123	0.144	0.431	0.250	0.152
connect-4	67557	42	2	0.405	0.389	0.326	0.258	0.394	0.389	0.371	0.155
contrac	1473	9	3	0.591	0.585	0.525	0.546	0.579	0.573	0.569	0.544
credit-approval	690	15	2	0.344	0.337	0.316	0.241	0.311	0.337	0.289	0.316
cylinder-bands	512	35	2	0.481	0.464	0.493	0.331	0.406	0.464	0.373	0.288
dermatology	366	34	6	0.603	0.572	0.573	0.046	0.194	0.607	0.317	0.121
echocardiogram	131	10	2	0.463	0.350	0.274	0.303	0.357	0.350	0.236	0.325
ecoli	336	7	8	0.409	0.396	0.443	0.244	0.259	0.344	0.251	0.251
energy-y1	768	8	3	0.442	0.333	0.258	0.163	0.165	0.312	0.165	0.211
energy-y2	768	8	3	0.481	0.409	0.479	0.298	0.260	0.396	0.290	0.307
fertility	100	9	2	0.218	0.200	0.180	0.153	0.165	0.200	0.121	0.098
flags	194	28	8	0.760	0.703	0.774	0.651	0.649	0.697	0.632	0.647
glass	214	9	6	0.564	0.501	0.637	0.480	0.385	0.462	0.471	0.384
haberman-survival	306	3	2	0.426	0.420	0.363	0.389	0.400	0.420	0.334	0.477
hayes-roth	160	3	3	0.672	0.560	0.796	0.569	0.537	0.553	0.649	0.510

Continued on next page.

Detecting Misclassification Errors in Neural Networks with a Gaussian Process Model

Dataset	N	M	K	RED	MCP	Trust Score	ConfidNet	Intro-Net	Entropy	DNGO	SVGP
heart-cleveland	303	13	5	0.752	0.739	0.694	0.675	0.694	0.719	0.612	0.720
heart-hungarian	294	12	2	0.406	0.388	0.416	0.234	0.360	0.388	0.326	0.317
heart-switzerland	123	12	5	0.720	0.672	0.711	0.677	0.639	0.680	0.685	0.618
heart-va	200	12	5	0.748	0.720	0.658	0.664	0.721	0.736	0.665	0.621
hepatitis	155	19	2	0.499	0.383	0.435	0.375	0.273	0.383	0.365	0.317
hill-valley	1212	100	2	0.654	0.540	0.472	0.502	0.591	0.541	0.545	0.540
horse-colic	368	25	2	0.422	0.407	0.399	0.245	0.369	0.407	0.289	0.225
ilpd-indian-liver	583	9	2	0.458	0.445	0.410	0.419	0.428	0.445	0.433	0.429
image-segmentation	2310	18	7	0.527	0.434	0.449	0.229	0.200	0.409	0.208	0.123
ionosphere	351	33	2	0.513	0.452	0.303	0.128	0.364	0.452	0.286	0.148
iris	150	4	3	0.623	0.553	0.684	0.105	0.173	0.511	0.337	0.189
led-display	1000	7	10	0.574	0.573	0.566	0.557	0.512	0.548	0.504	0.469
lenses	24	4	3	0.833	0.887	0.798	0.572	0.759	0.887	0.530	0.499
letter	20000	16	26	0.493	0.459	0.784	0.242	0.125	0.463	0.110	0.162
libras	360	90	15	0.586	0.485	0.639	0.287	0.282	0.449	0.482	0.258
low-res-spect	531	100	9	0.536	0.493	0.437	0.281	0.288	0.479	0.274	0.314
lung-cancer	32	56	3	0.870	0.784	0.609	0.633	0.812	0.836	0.572	0.479
lymphography	148	18	4	0.641	0.512	0.582	0.228	0.339	0.514	0.302	0.323
magic	19020	10	2	0.364	0.353	0.293	0.307	0.348	0.353	0.293	0.232
mammographic	961	5	2	0.458	0.456	0.277	0.399	0.441	0.456	0.402	0.384
messidor	1151	19	2	0.458	0.442	0.350	0.356	0.417	0.442	0.404	0.341
miniboone	130064	50	2	0.379	0.361	0.190	0.299	0.370	0.361	0.349	0.162
molec-biol-promoter	106	57	2	0.506	0.497	0.765	0.292	0.436	0.497	0.399	0.396
molec-biol-splice	3190	60	3	0.457	0.450	0.372	0.189	0.203	0.459	0.398	0.171
monks-1	556	6	2	0.576	0.359	0.126	0.199	0.305	0.359	0.153	0.149
monks-2	601	6	2	0.512	0.452	0.622	0.405	0.412	0.452	0.376	0.374
monks-3	554	6	2	0.603	0.509	0.290	0.269	0.403	0.509	0.450	0.123
mushroom	8124	21	2	NA	NA	NA	NA	NA	NA	NA	NA
musk-1	476	166	2	0.482	0.470	0.476	0.081	0.319	0.470	0.273	0.089
musk-2	6598	166	2	0.371	0.339	0.064	0.007	0.061	0.339	0.503	0.006
nursery	12960	8	5	0.550	0.388	0.070	0.027	0.129	0.386	0.368	0.131
oocytes_merluccius_nucleus_4d	1022	41	2	0.431	0.389	0.264	0.284	0.368	0.389	0.378	0.318
oocytes_merluccius_states_2f	1022	25	3	0.486	0.466	0.387	0.234	0.338	0.453	0.304	0.244
oocytes_trisopterus_nucleus_2f	912	25	2	0.470	0.439	0.329	0.262	0.447	0.439	0.349	0.285
oocytes_trisopterus_states_5b	912	32	3	0.420	0.394	0.321	0.137	0.266	0.417	0.316	0.101
optical	5620	62	10	0.437	0.411	0.572	0.043	0.037	0.402	0.070	0.067
ozone	2536	72	2	0.288	0.269	0.253	0.189	0.127	0.269	0.516	0.023
page-blocks	5473	10	5	0.439	0.374	0.388	0.317	0.263	0.359	0.255	0.173
parkinsons	195	22	2	0.490	0.456	0.477	0.108	0.197	0.456	0.264	0.277
pendigits	10992	16	10	0.480	0.344	0.677	0.168	0.124	0.343	0.102	0.050
phishing	1353	9	3	0.439	0.416	0.357	0.332	0.355	0.399	0.330	0.322
pima	768	8	2	0.489	0.480	0.408	0.399	0.477	0.480	0.414	0.322
pittsburg-bridges-MATERIAL	106	7	3	0.553	0.444	0.405	0.308	0.459	0.449	0.272	0.336
pittsburg-bridges-REL-L	103	7	3	0.565	0.498	0.624	0.485	0.519	0.491	0.464	0.452
pittsburg-bridges-SPAN	92	7	3	0.536	0.504	0.494	0.319	0.461	0.521	0.416	0.412
pittsburg-bridges-T-OR-D	102	7	2	0.388	0.299	0.376	0.320	0.462	0.299	0.298	0.274
pittsburg-bridges-TYPE	105	7	6	0.797	0.713	0.741	0.658	0.634	0.664	0.668	0.716
planning	182	12	2	0.339	0.337	0.362	0.315	0.295	0.337	0.281	0.229
plant-margin	1600	64	100	0.580	0.565	0.692	0.323	0.258	0.562	0.297	0.179
plant-shape	1600	64	100	0.690	0.662	0.757	0.519	0.475	0.639	0.513	0.472
plant-texture	1599	64	100	0.602	0.590	0.704	0.300	0.323	0.605	0.275	0.216
post-operative	90	8	3	0.391	0.375	0.230	0.329	0.368	0.334	0.398	0.368
primary-tumor	330	17	15	0.789	0.777	0.683	0.717	0.712	0.772	0.673	0.704
ringnorm	7400	20	2	0.334	0.329	0.269	0.040	0.111	0.329	0.285	0.025
seeds	210	7	3	0.515	0.447	0.453	0.282	0.284	0.405	0.340	0.314
semeion	1593	256	10	0.530	0.514	0.698	0.083	0.224	0.554	0.166	0.132
soybean	683	35	18	0.546	0.476	0.418	0.282	0.164	0.469	0.209	0.289
spambase	4601	57	2	0.307	0.282	0.290	0.170	0.228	0.282	0.211	0.131
spect	265	22	2	0.503	0.487	0.381	0.425	0.451	0.487	0.397	0.419
spectf	267	44	2	0.447	0.386	0.395	0.216	0.392	0.387	0.286	0.304
statlog-australian-credit	690	14	2	0.465	0.446	0.408	0.408	0.406	0.446	0.395	0.421
statlog-german-credit	1000	24	2	0.413	0.410	0.373	0.320	0.378	0.410	0.352	0.244
statlog-heart	270	13	2	0.443	0.406	0.351	0.288	0.435	0.406	0.329	0.255
statlog-image	2310	18	7	0.541	0.437	0.465	0.220	0.100	0.452	0.260	0.166
statlog-landsat	6435	36	6	0.425	0.393	0.551	0.317	0.306	0.404	0.291	0.251
statlog-shuttle	58000	9	7	0.534	0.294	0.527	0.214	0.183	0.281	0.347	0.229
statlog-vehicle	846	18	4	0.531	0.515	0.304	0.376	0.347	0.524	0.335	0.350
steel-plates	1941	27	7	0.523	0.511	0.528	0.446	0.430	0.508	0.432	0.397
synthetic-control	600	60	6	0.590	0.453	0.396	0.031	0.076	0.402	0.209	0.020
teaching	151	5	3	0.626	0.578	0.503	0.614	0.568	0.586	0.653	0.544
thyroid	7200	21	3	0.428	0.397	0.148	0.116	0.178	0.390	0.508	0.101
tic-tac-toe	958	9	2	0.562	0.473	1.000	0.132	0.461	0.473	0.423	0.418
titanic	2201	3	2	0.386	0.385	0.599	0.372	0.386	0.385	0.437	0.370
trains	10	29	2	0.667	0.625	0.875	0.750	0.625	0.625	0.438	0.625
twonorm	7400	20	2	0.359	0.345	0.394	0.152	0.278	0.345	0.270	0.034
vertebral-column-2clases	310	6	2	0.468	0.456	0.302	0.345	0.402	0.456	0.349	0.243
vertebral-column-3clases	310	6	3	0.505	0.478	0.279	0.460	0.366	0.495	0.411	0.271

Continued on next page.

Detecting Misclassification Errors in Neural Networks with a Gaussian Process Model

Dataset	N	M	K	RED	MCP	Trust Score	ConfidNet	Intro-Net	Entropy	DNGO	SVGP
wall-following	5456	24	4	0.414	0.373	0.299	0.204	0.243	0.364	0.263	0.135
waveform	5000	21	3	0.462	0.419	0.327	0.353	0.390	0.419	0.537	0.159
waveform-noise	5000	40	3	0.424	0.394	0.318	0.227	0.322	0.394	0.511	0.165
wine	178	13	3	0.857	0.669	0.606	0.056	0.413	0.794	0.602	0.181
wine-quality-red	1599	11	6	0.530	0.518	0.537	0.489	0.486	0.491	0.519	0.448
wine-quality-white	4898	11	7	0.539	0.527	0.625	0.532	0.521	0.514	0.523	0.478
yeast	1484	8	10	0.565	0.557	0.506	0.502	0.493	0.542	0.405	0.911
zoo	101	16	7	0.888	0.744	0.752	0.183	0.473	0.842	0.385	0.657

Continued from previous page.

Table 8: Comparison between RED and Counterparts Using AUPR-Success

Dataset	N	M	K	RED	MCP	Trust Score	ConfidNet	Intro-Net	Entropy	DNGO	SVGP
abalone	4177	8	3	0.852	0.850	0.821	0.844	0.844	0.849	0.806	0.840
acute-inflammation	120	6	2	NA	NA	NA	NA	NA	NA	NA	NA
acute-nephritis	120	6	2	NA	NA	NA	NA	NA	NA	NA	NA
adult	48842	14	2	0.968	0.967	0.944	0.964	0.961	0.967	0.897	0.961
annealing	898	31	5	0.975	0.903	0.942	0.907	0.914	0.899	0.908	0.919
arrhythmia	452	262	13	0.814	0.806	0.806	0.645	0.659	0.799	0.665	0.775
audiology-std	196	59	18	0.945	0.925	NA	0.609	0.725	0.925	0.741	0.769
balance-scale	625	4	3	0.999	0.999	0.997	0.971	0.983	0.999	0.986	0.976
balloons	16	4	2	0.773	0.736	0.861	0.690	0.736	0.736	0.516	0.542
bank	4521	16	2	0.977	0.980	0.976	0.968	0.936	0.980	0.946	0.979
biocconcentration	779	9	3	0.742	0.723	0.779	0.712	0.722	0.716	0.687	0.693
blood	748	4	2	0.891	0.891	0.872	0.901	0.882	0.891	0.881	0.899
breast-cancer	286	9	2	0.815	0.814	0.757	0.788	0.767	0.814	0.758	0.777
breast-cancer-wisc	699	9	2	0.998	0.997	0.998	0.994	0.984	0.997	0.992	0.986
breast-cancer-wisc-diag	569	30	2	0.996	0.997	0.997	0.969	0.980	0.998	0.970	0.981
breast-cancer-wisc-prog	198	33	2	0.850	0.855	0.787	0.817	0.828	0.855	0.779	0.785
breast-tissue	106	9	6	0.902	0.869	0.893	0.855	0.751	0.863	0.782	0.838
car	1728	6	4	0.999	0.999	0.999	0.992	0.988	0.999	0.989	0.989
cardiotocography-10clases	2126	21	10	0.959	0.959	0.927	0.889	0.871	0.958	0.884	0.901
cardiotocography-3clases	2126	21	3	0.990	0.991	0.988	0.971	0.963	0.991	0.963	0.979
chess-krvk	28056	6	18	0.900	0.890	0.934	0.867	0.837	0.889	0.782	0.801
chess-krvkp	3196	36	2	1.000	1.000	0.995	0.990	0.994	1.000	0.972	0.996
climate	540	20	2	0.991	0.989	0.976	0.937	0.975	0.986	0.958	0.949
congressional-voting	435	16	2	0.701	0.701	0.706	0.704	0.694	0.701	0.713	0.698
conn-bench-sonar-mines-rocks	208	60	2	0.961	0.963	0.980	0.806	0.898	0.963	0.852	0.894
conn-bench-vowel-deterding	990	11	11	1.000	1.000	1.000	0.979	0.984	1.000	0.991	0.989
connect-4	67557	42	2	0.969	0.969	0.938	0.942	0.958	0.969	0.883	0.867
contrac	1473	9	3	0.716	0.713	0.578	0.680	0.672	0.704	0.654	0.667
credit-approval	690	15	2	0.942	0.941	0.915	0.908	0.936	0.941	0.888	0.927
cylinder-bands	512	35	2	0.864	0.860	0.870	0.784	0.804	0.860	0.769	0.752
dermatology	366	34	6	0.999	0.999	0.997	0.975	0.980	0.999	0.976	0.950
echocardiogram	131	10	2	0.941	0.934	0.922	0.913	0.920	0.934	0.881	0.925
ecoli	336	7	8	0.958	0.955	0.969	0.908	0.874	0.953	0.881	0.916
energy-y1	768	8	3	0.992	0.993	0.992	0.975	0.973	0.993	0.960	0.983
energy-y2	768	8	3	0.986	0.986	0.985	0.961	0.945	0.986	0.960	0.978
fertility	100	9	2	0.951	0.923	0.946	0.914	0.924	0.923	0.893	0.936
flags	194	28	8	0.731	0.707	0.812	0.551	0.599	0.710	0.560	0.585
glass	214	9	6	0.850	0.804	0.912	0.767	0.725	0.802	0.729	0.775
haberman-survival	306	3	2	0.844	0.843	0.851	0.815	0.828	0.843	0.813	0.829
hayes-roth	160	3	3	0.932	0.880	0.965	0.882	0.854	0.885	0.864	0.821
heart-cleveland	303	13	5	0.853	0.856	0.832	0.792	0.818	0.858	0.683	0.835
heart-hungarian	294	12	2	0.923	0.905	0.926	0.841	0.912	0.905	0.838	0.862
heart-switzerland	123	12	5	0.464	0.440	0.429	0.399	0.414	0.448	0.435	0.408
heart-va	200	12	5	0.500	0.470	0.438	0.413	0.480	0.483	0.390	0.364
hepatitis	155	19	2	0.964	0.964	0.974	0.925	0.888	0.964	0.891	0.910
hill-valley	1212	100	2	0.761	0.702	0.554	0.650	0.739	0.702	0.702	0.690
horse-colic	368	25	2	0.926	0.916	0.917	0.827	0.911	0.916	0.825	0.869
ilpd-indian-liver	583	9	2	0.878	0.873	0.811	0.859	0.862	0.873	0.816	0.869
image-segmentation	2310	18	7	0.997	0.997	0.998	0.983	0.984	0.997	0.977	0.985
ionosphere	351	33	2	0.990	0.988	0.976	0.897	0.973	0.988	0.928	0.933
iris	150	4	3	0.992	0.991	0.997	0.935	0.912	0.990	0.945	0.954
led-display	1000	7	10	0.888	0.888	0.773	0.877	0.849	0.885	0.824	0.845
lenses	24	4	3	0.979	0.947	0.944	0.831	0.845	0.947	0.818	0.815
letter	20000	16	26	0.995	0.996	0.999	0.980	0.888	0.996	0.964	0.982
libras	360	90	15	0.955	0.942	0.955	0.802	0.800	0.940	0.859	0.848
low-res-spect	531	100	9	0.977	0.968	0.952	0.905	0.889	0.968	0.898	0.949
lung-cancer	32	56	3	0.728	0.687	0.572	0.461	0.703	0.688	0.393	0.356
lymphography	148	18	4	0.939	0.922	0.956	0.797	0.851	0.921	0.856	0.817
magic	19020	10	2	0.966	0.966	0.954	0.960	0.959	0.966	0.838	0.946
mammographic	961	5	2	0.922	0.918	0.881	0.909	0.910	0.918	0.865	0.925
messidor	1151	19	2	0.862	0.861	0.762	0.805	0.829	0.861	0.795	0.805

Continued on next page.

Detecting Misclassification Errors in Neural Networks with a Gaussian Process Model

Dataset	N	M	K	RED	MCP	Trust Score	ConfidNet	Intro-Net	Entropy	DNGO	SVGP
miniboone	130064	50	2	0.992	0.992	0.983	0.988	0.986	0.992	0.933	0.981
molec-biol-promoter	106	57	2	0.886	0.882	0.951	0.702	0.873	0.882	0.766	0.811
molec-biol-splice	3190	60	3	0.953	0.953	0.926	0.832	0.845	0.952	0.892	0.837
monks-1	556	6	2	0.998	0.997	0.982	0.988	0.989	0.997	0.983	0.995
monks-2	601	6	2	0.884	0.855	0.925	0.806	0.807	0.855	0.751	0.806
monks-3	554	6	2	0.999	0.999	0.992	0.980	0.993	0.999	0.977	0.991
mushroom	8124	21	2	NA	NA	NA	NA	NA	NA	NA	NA
musk-1	476	166	2	0.984	0.983	0.986	0.910	0.956	0.983	0.909	0.934
musk-2	6598	166	2	1.000	1.000	0.998	0.995	0.995	1.000	0.997	0.994
nursery	12960	8	5	1.000	1.000	1.000	0.999	0.999	1.000	0.999	1.000
oocytes_merluccius_nucleus_4d	1022	41	2	0.939	0.929	0.881	0.891	0.903	0.929	0.881	0.907
oocytes_merluccius_states_2f	1022	25	3	0.991	0.991	0.991	0.967	0.970	0.991	0.952	0.975
oocytes_trisopterus_nucleus_2f	912	25	2	0.939	0.931	0.907	0.870	0.922	0.931	0.858	0.874
oocytes_trisopterus_states_5b	912	32	3	0.991	0.990	0.985	0.951	0.967	0.990	0.932	0.945
optical	5620	62	10	0.999	0.999	0.999	0.981	0.978	0.999	0.980	0.992
ozone	2536	72	2	0.994	0.996	0.993	0.988	0.966	0.996	0.984	0.951
page-blocks	5473	10	5	0.998	0.997	0.993	0.993	0.989	0.997	0.966	0.994
parkinsons	195	22	2	0.994	0.992	0.995	0.936	0.942	0.992	0.960	0.963
pendigits	10992	16	10	0.999	0.999	1.000	0.992	0.992	0.999	0.994	0.993
phishing	1353	9	3	0.975	0.973	0.958	0.959	0.945	0.972	0.919	0.952
pima	768	8	2	0.897	0.893	0.873	0.845	0.871	0.893	0.839	0.869
pittsburg-bridges-MATERIAL	106	7	3	0.975	0.968	0.950	0.916	0.928	0.968	0.881	0.936
pittsburg-bridges-REL-L	103	7	3	0.776	0.766	0.832	0.741	0.725	0.769	0.715	0.755
pittsburg-bridges-SPAN	92	7	3	0.842	0.793	0.766	0.649	0.734	0.790	0.767	0.695
pittsburg-bridges-T-OR-D	102	7	2	0.956	0.941	0.919	0.924	0.945	0.941	0.931	0.916
pittsburg-bridges-TYPE	105	7	6	0.805	0.658	0.718	0.612	0.596	0.631	0.713	0.748
planning	182	12	2	0.715	0.709	0.723	0.714	0.713	0.709	0.720	0.677
plant-margin	1600	64	100	0.951	0.949	0.966	0.827	0.816	0.950	0.815	0.729
plant-shape	1600	64	100	0.860	0.849	0.879	0.715	0.668	0.837	0.693	0.669
plant-texture	1599	64	100	0.953	0.950	0.958	0.807	0.780	0.950	0.786	0.790
post-operative	90	8	3	0.653	0.642	0.719	0.656	0.660	0.639	0.702	0.654
primary-tumor	330	17	15	0.757	0.746	0.646	0.627	0.623	0.745	0.531	0.629
ringnorm	7400	20	2	0.999	0.999	0.989	0.982	0.977	0.999	0.959	0.976
seeds	210	7	3	0.987	0.986	0.991	0.962	0.960	0.985	0.929	0.945
semeion	1593	256	10	0.994	0.994	0.996	0.926	0.949	0.994	0.943	0.963
soybean	683	35	18	0.996	0.995	0.993	0.970	0.940	0.995	0.942	0.973
spambase	4601	57	2	0.989	0.988	0.983	0.965	0.966	0.988	0.941	0.974
spect	265	22	2	0.805	0.795	0.762	0.721	0.783	0.795	0.673	0.724
spectf	267	44	2	0.954	0.951	0.941	0.911	0.917	0.952	0.880	0.948
statlog-australian-credit	690	14	2	0.696	0.687	0.649	0.662	0.672	0.687	0.621	0.657
statlog-german-credit	1000	24	2	0.889	0.890	0.872	0.835	0.848	0.890	0.771	0.779
statlog-heart	270	13	2	0.939	0.934	0.904	0.878	0.914	0.934	0.829	0.860
statlog-image	2310	18	7	0.998	0.998	0.998	0.986	0.979	0.998	0.984	0.990
statlog-landsat	6435	36	6	0.986	0.987	0.991	0.963	0.959	0.987	0.948	0.971
statlog-shuttle	58000	9	7	1.000	1.000	1.000	0.998	0.907	0.999	0.999	0.999
statlog-vehicle	846	18	4	0.965	0.967	0.927	0.928	0.912	0.968	0.868	0.921
steel-plates	1941	27	7	0.919	0.916	0.928	0.881	0.848	0.915	0.824	0.870
synthetic-control	600	60	6	1.000	1.000	0.999	0.985	0.988	1.000	0.987	0.986
teaching	151	5	3	0.668	0.625	0.569	0.630	0.625	0.611	0.662	0.615
thyroid	7200	21	3	0.999	0.999	0.996	0.992	0.984	0.999	0.992	0.996
tic-tac-toe	958	9	2	1.000	0.999	1.000	0.999	0.998	0.999	0.994	0.999
titanic	2201	3	2	0.895	0.894	0.889	0.890	0.891	0.894	0.878	0.895
trains	10	29	2	0.667	0.625	0.875	0.750	0.625	0.625	0.438	0.625
twonorm	7400	20	2	0.998	0.999	0.998	0.991	0.991	0.999	0.924	0.973
vertebral-column-2classes	310	6	2	0.977	0.977	0.952	0.952	0.940	0.977	0.894	0.936
vertebral-column-3classes	310	6	3	0.977	0.977	0.943	0.958	0.931	0.977	0.908	0.952
wall-following	5456	24	4	0.980	0.980	0.972	0.928	0.949	0.980	0.941	0.932
waveform	5000	21	3	0.968	0.966	0.947	0.947	0.940	0.966	0.928	0.847
waveform-noise	5000	40	3	0.962	0.962	0.935	0.880	0.900	0.962	0.926	0.844
wine	178	13	3	0.999	0.999	0.998	0.945	0.990	0.999	0.968	0.978
wine-quality-red	1599	11	6	0.734	0.726	0.750	0.702	0.692	0.717	0.692	0.695
wine-quality-white	4898	11	7	0.672	0.662	0.745	0.648	0.654	0.655	0.650	0.610
yeast	1484	8	10	0.754	0.749	0.704	0.716	0.689	0.742	0.598	0.571
zoo	101	16	7	0.999	0.997	0.997	0.919	0.958	0.999	0.958	0.943

Continued from previous page.

Table 9: Comparison between RED and Counterparts Using AUROC

Dataset	N	M	K	RED	MCP	Trust Score	ConfidNet	Intro-Net	Entropy	DNGO	SVGP
abalone	4177	8	3	0.734	0.730	0.680	0.719	0.726	0.726	0.697	0.700
acute-inflammation	120	6	2	NA	NA	NA	NA	NA	NA	NA	NA
acute-nephritis	120	6	2	NA	NA	NA	NA	NA	NA	NA	NA
adult	48842	14	2	0.841	0.837	0.759	0.828	0.830	0.837	0.751	0.814
annealing	898	31	5	0.865	0.699	0.776	0.724	0.723	0.694	0.619	0.675

Continued on next page.

Detecting Misclassification Errors in Neural Networks with a Gaussian Process Model

Dataset	N	M	K	RED	MCP	Trust Score	ConfidNet	Intro-Net	Entropy	DNGO	SVGP
arrhythmia	452	262	13	0.712	0.715	0.727	0.505	0.517	0.703	0.528	0.639
audiology-std	196	59	18	0.883	0.848	NA	0.439	0.605	0.852	0.666	0.672
balance-scale	625	4	3	0.986	0.987	0.909	0.510	0.621	0.985	0.712	0.536
balloons	16	4	2	0.741	0.667	0.722	0.556	0.667	0.667	0.312	0.333
bank	4521	16	2	0.854	0.861	0.840	0.822	0.750	0.861	0.500	0.854
bioconcentration	779	9	3	0.621	0.607	0.660	0.572	0.595	0.588	0.547	0.541
blood	748	4	2	0.705	0.705	0.634	0.716	0.687	0.705	0.665	0.704
breast-cancer	286	9	2	0.682	0.677	0.587	0.637	0.609	0.677	0.607	0.620
breast-cancer-wisc	699	9	2	0.944	0.936	0.945	0.873	0.759	0.936	0.797	0.727
breast-cancer-wisc-diag	569	30	2	0.925	0.925	0.921	0.558	0.682	0.940	0.551	0.575
breast-cancer-wisc-prog	198	33	2	0.640	0.644	0.521	0.566	0.595	0.644	0.514	0.484
breast-tissue	106	9	6	0.864	0.815	0.850	0.788	0.651	0.811	0.761	0.785
car	1728	6	4	0.974	0.968	0.934	0.717	0.615	0.968	0.653	0.691
cardiotocography-10clases	2126	21	10	0.839	0.835	0.756	0.670	0.622	0.829	0.660	0.663
cardiotocography-3clases	2126	21	3	0.902	0.901	0.882	0.804	0.761	0.900	0.563	0.813
chess-krvk	28056	6	18	0.778	0.759	0.868	0.722	0.685	0.753	0.616	0.642
chess-krvkp	3196	36	2	0.967	0.963	0.777	0.573	0.642	0.963	0.568	0.688
climate	540	20	2	0.898	0.858	0.760	0.449	0.744	0.854	0.554	0.572
congressional-voting	435	16	2	0.603	0.600	0.562	0.607	0.595	0.598	0.619	0.612
conn-bench-sonar-mines-rocks	208	60	2	0.833	0.833	0.912	0.488	0.643	0.833	0.634	0.625
conn-bench-vowel-deterding	990	11	11	0.990	0.979	0.995	0.582	0.624	0.979	0.716	0.759
connect-4	67557	42	2	0.836	0.831	0.744	0.727	0.816	0.831	0.736	0.522
contrac	1473	9	3	0.663	0.658	0.556	0.619	0.642	0.645	0.626	0.608
credit-approval	690	15	2	0.741	0.741	0.683	0.649	0.703	0.741	0.625	0.694
cylinder-bands	512	35	2	0.703	0.702	0.713	0.579	0.637	0.702	0.561	0.516
dermatology	366	34	6	0.980	0.974	0.934	0.589	0.766	0.976	0.750	0.333
echocardiogram	131	10	2	0.758	0.709	0.655	0.634	0.687	0.709	0.597	0.659
ecoli	336	7	8	0.791	0.785	0.806	0.670	0.556	0.773	0.592	0.667
energy-y1	768	8	3	0.896	0.886	0.848	0.691	0.650	0.886	0.604	0.777
energy-y2	768	8	3	0.892	0.880	0.874	0.777	0.668	0.880	0.802	0.834
fertility	100	9	2	0.588	0.469	0.563	0.382	0.485	0.469	0.413	0.508
flags	194	28	8	0.727	0.696	0.791	0.603	0.618	0.698	0.598	0.574
glass	214	9	6	0.719	0.659	0.823	0.648	0.560	0.651	0.603	0.581
haberman-survival	306	3	2	0.694	0.692	0.651	0.645	0.671	0.692	0.636	0.684
hayes-roth	160	3	3	0.846	0.746	0.909	0.785	0.749	0.759	0.811	0.674
heart-cleveland	303	13	5	0.806	0.811	0.783	0.758	0.769	0.811	0.680	0.786
heart-hungarian	294	12	2	0.750	0.724	0.742	0.555	0.730	0.724	0.599	0.650
heart-switzerland	123	12	5	0.584	0.545	0.580	0.545	0.496	0.554	0.554	0.499
heart-va	200	12	5	0.629	0.606	0.544	0.522	0.603	0.618	0.505	0.455
hepatitis	155	19	2	0.822	0.797	0.845	0.703	0.619	0.797	0.624	0.677
hill-valley	1212	100	2	0.712	0.636	0.512	0.585	0.669	0.636	0.636	0.627
horse-colic	368	25	2	0.743	0.731	0.749	0.530	0.717	0.731	0.563	0.568
ilpd-indian-liver	583	9	2	0.719	0.709	0.650	0.686	0.695	0.709	0.614	0.709
image-segmentation	2310	18	7	0.935	0.936	0.946	0.770	0.742	0.935	0.734	0.749
ionosphere	351	33	2	0.909	0.886	0.779	0.504	0.786	0.886	0.630	0.535
iris	150	4	3	0.942	0.928	0.963	0.553	0.471	0.926	0.693	0.612
led-display	1000	7	10	0.762	0.762	0.545	0.749	0.717	0.753	0.706	0.700
lenses	24	4	3	0.917	0.875	0.863	0.677	0.740	0.875	0.625	0.583
letter	20000	16	26	0.932	0.940	0.977	0.795	0.526	0.940	0.646	0.775
libras	360	90	15	0.845	0.812	0.865	0.524	0.535	0.803	0.681	0.562
low-res-spect	531	100	9	0.864	0.837	0.791	0.618	0.559	0.836	0.616	0.717
lung-cancer	32	56	3	0.759	0.686	0.573	0.444	0.700	0.725	0.378	0.304
lymphography	148	18	4	0.805	0.753	0.825	0.503	0.622	0.748	0.623	0.566
magic	19020	10	2	0.810	0.807	0.753	0.788	0.796	0.807	0.639	0.720
mammographic	961	5	2	0.764	0.761	0.650	0.729	0.742	0.761	0.693	0.755
messidor	1151	19	2	0.697	0.690	0.565	0.609	0.662	0.690	0.646	0.601
miniboone	130064	50	2	0.905	0.903	0.806	0.878	0.882	0.903	0.781	0.783
molec-biol-promoter	106	57	2	0.735	0.727	0.885	0.414	0.719	0.727	0.505	0.576
molec-biol-splice	3190	60	3	0.810	0.810	0.722	0.517	0.547	0.811	0.717	0.501
monks-1	556	6	2	0.959	0.936	0.619	0.715	0.779	0.936	0.597	0.862
monks-2	601	6	2	0.751	0.698	0.814	0.616	0.632	0.698	0.602	0.598
monks-3	554	6	2	0.972	0.966	0.845	0.750	0.872	0.966	0.820	0.825
mushroom	8124	21	2	NA	NA	NA	NA	NA	NA	NA	NA
musk-1	476	166	2	0.863	0.860	0.863	0.449	0.724	0.860	0.635	0.503
musk-2	6598	166	2	0.984	0.981	0.794	0.513	0.627	0.982	0.500	0.417
nursery	12960	8	5	0.993	0.955	0.925	0.601	0.603	0.965	0.674	0.832
oocytes_merluccius_nucleus_4d	1022	41	2	0.779	0.758	0.627	0.652	0.717	0.758	0.708	0.693
oocytes_merluccius_states_2f	1022	25	3	0.907	0.909	0.907	0.763	0.795	0.908	0.706	0.793
oocytes_trisopterus_nucleus_2f	912	25	2	0.786	0.766	0.693	0.619	0.759	0.766	0.665	0.638
oocytes_trisopterus_states_5b	912	32	3	0.898	0.895	0.834	0.638	0.744	0.895	0.704	0.546
optical	5620	62	10	0.970	0.964	0.973	0.561	0.534	0.964	0.573	0.703
ozone	2536	72	2	0.899	0.905	0.851	0.773	0.568	0.906	0.500	0.315
page-blocks	5473	10	5	0.952	0.942	0.905	0.906	0.855	0.941	0.792	0.861
parkinsons	195	22	2	0.918	0.881	0.928	0.574	0.561	0.881	0.729	0.666
pendigits	10992	16	10	0.951	0.948	0.972	0.681	0.635	0.947	0.650	0.660
phishing	1353	9	3	0.859	0.852	0.788	0.798	0.762	0.847	0.726	0.766
pima	768	8	2	0.754	0.751	0.700	0.673	0.730	0.751	0.697	0.653

Continued on next page.

Detecting Misclassification Errors in Neural Networks with a Gaussian Process Model

Dataset	N	M	K	RED	MCP	Trust Score	ConfidNet	Intro-Net	Entropy	DNGO	SVGP
pittsburg-bridges-MATERIAL	106	7	3	0.848	0.771	0.776	0.586	0.706	0.772	0.535	0.692
pittsburg-bridges-REL-L	103	7	3	0.643	0.611	0.739	0.612	0.587	0.614	0.569	0.604
pittsburg-bridges-SPAN	92	7	3	0.689	0.634	0.631	0.403	0.574	0.631	0.579	0.488
pittsburg-bridges-T-OR-D	102	7	2	0.778	0.740	0.694	0.669	0.750	0.740	0.712	0.653
pittsburg-bridges-TYPE	105	7	6	0.799	0.713	0.743	0.657	0.636	0.673	0.723	0.728
planning	182	12	2	0.479	0.468	0.509	0.492	0.473	0.468	0.474	0.400
plant-margin	1600	64	100	0.846	0.844	0.888	0.605	0.559	0.844	0.583	0.391
plant-shape	1600	64	100	0.794	0.780	0.823	0.647	0.587	0.760	0.626	0.586
plant-texture	1599	64	100	0.854	0.848	0.883	0.580	0.560	0.850	0.534	0.491
post-operative	90	8	3	0.443	0.433	0.414	0.433	0.446	0.410	0.517	0.480
primary-tumor	330	17	15	0.769	0.765	0.676	0.689	0.673	0.764	0.621	0.689
ringnorm	7400	20	2	0.953	0.952	0.708	0.587	0.565	0.952	0.623	0.507
seeds	210	7	3	0.913	0.890	0.913	0.746	0.724	0.881	0.717	0.610
semeion	1593	256	10	0.930	0.926	0.953	0.499	0.662	0.928	0.615	0.657
soybean	683	35	18	0.945	0.942	0.916	0.765	0.598	0.937	0.614	0.807
spambase	4601	57	2	0.864	0.856	0.809	0.710	0.724	0.856	0.692	0.713
spect	265	22	2	0.668	0.660	0.581	0.562	0.620	0.660	0.524	0.558
spectf	267	44	2	0.798	0.788	0.740	0.650	0.727	0.789	0.621	0.760
statlog-australian-credit	690	14	2	0.585	0.569	0.543	0.537	0.539	0.569	0.510	0.525
statlog-german-credit	1000	24	2	0.715	0.720	0.679	0.620	0.676	0.720	0.636	0.513
statlog-heart	270	13	2	0.762	0.746	0.693	0.624	0.731	0.746	0.580	0.565
statlog-image	2310	18	7	0.943	0.947	0.941	0.818	0.683	0.947	0.777	0.784
statlog-landsat	6435	36	6	0.888	0.887	0.919	0.795	0.770	0.889	0.755	0.787
statlog-shuttle	58000	9	7	0.995	0.919	0.998	0.763	0.589	0.911	0.599	0.778
statlog-vehicle	846	18	4	0.854	0.856	0.719	0.759	0.716	0.858	0.682	0.730
steel-plates	1941	27	7	0.795	0.790	0.805	0.736	0.695	0.787	0.688	0.692
synthetic-control	600	60	6	0.984	0.980	0.956	0.497	0.547	0.977	0.671	0.497
teaching	151	5	3	0.645	0.596	0.555	0.618	0.574	0.585	0.662	0.553
thyroid	7200	21	3	0.970	0.963	0.849	0.782	0.646	0.968	0.500	0.809
tic-tac-toe	958	9	2	0.986	0.933	1.000	0.876	0.894	0.933	0.684	0.942
titanic	2201	3	2	0.673	0.671	0.508	0.662	0.671	0.671	0.553	0.674
trains	10	29	2	0.556	0.500	0.833	0.667	0.500	0.500	0.250	0.500
twonorm	7400	20	2	0.952	0.952	0.941	0.817	0.812	0.952	0.662	0.499
vertebral-column-2clases	310	6	2	0.860	0.857	0.770	0.771	0.765	0.857	0.735	0.707
vertebral-column-3clases	310	6	3	0.877	0.873	0.715	0.819	0.710	0.877	0.726	0.750
wall-following	5456	24	4	0.850	0.847	0.793	0.641	0.706	0.846	0.700	0.603
waveform	5000	21	3	0.846	0.834	0.761	0.773	0.791	0.833	0.563	0.500
waveform-noise	5000	40	3	0.823	0.819	0.727	0.601	0.692	0.818	0.581	0.505
wine	178	13	3	0.991	0.975	0.954	0.345	0.799	0.980	0.751	0.646
wine-quality-red	1599	11	6	0.647	0.638	0.644	0.615	0.607	0.617	0.625	0.573
wine-quality-white	4898	11	7	0.621	0.612	0.677	0.604	0.605	0.597	0.600	0.553
yeast	1484	8	10	0.683	0.678	0.620	0.627	0.611	0.665	0.486	0.792
zoo	101	16	7	0.986	0.970	0.958	0.659	0.779	0.987	0.594	0.783

Continued from previous page.

Table 10: Comparison between RED and Counterparts Using AP-Error

Dataset	N	M	K	RED+BNN	BNN MCP	BNN Entropy	RED+MC-D	MC-D MCP	MC-D Entropy
abalone	4177	8	3	0.529	0.522	0.513	0.516	0.509	0.503
acute-inflammation	120	6	2	NA	NA	NA	NA	NA	NA
acute-nephritis	120	6	2	NA	NA	NA	NA	NA	NA
adult	48842	14	2	0.415	0.407	0.406	0.416	0.405	0.405
annealing	898	31	5	0.788	0.424	0.338	0.590	0.421	0.375
arrhythmia	452	262	13	0.719	0.614	0.734	0.551	0.543	0.540
audiology-std	196	59	18	0.768	0.684	0.756	0.760	0.659	0.698
balance-scale	625	4	3	0.820	0.532	0.581	0.685	0.548	0.621
balloons	16	4	2	0.825	0.810	0.810	0.852	0.824	0.824
bank	4521	16	2	0.527	0.443	0.448	0.431	0.410	0.413
bioconcentration	779	9	3	0.562	0.487	0.486	0.462	0.440	0.418
blood	748	4	2	0.515	0.471	0.498	0.441	0.441	0.443
breast-cancer	286	9	2	0.504	0.396	0.421	0.518	0.486	0.497
breast-cancer-wisc	699	9	2	0.512	0.473	0.447	0.454	0.425	0.418
breast-cancer-wisc-diag	569	30	2	0.430	0.362	0.446	0.545	0.476	0.543
breast-cancer-wisc-prog	198	33	2	0.553	0.491	0.521	0.504	0.497	0.491
breast-tissue	106	9	6	0.847	0.777	0.797	0.885	0.841	0.832
car	1728	6	4	0.604	0.495	0.339	0.656	0.480	0.326
cardiotocography-10clases	2126	21	10	0.548	0.515	0.463	0.529	0.488	0.464
cardiotocography-3clases	2126	21	3	0.499	0.424	0.421	0.468	0.400	0.405
chess-krvk	28056	6	18	0.514	0.501	0.474	0.751	0.675	0.648
chess-krvkp	3196	36	2	0.392	0.369	0.385	0.443	0.417	0.424
climate	540	20	2	0.553	0.506	0.532	0.442	0.416	0.472
congressional-voting	435	16	2	0.517	0.466	0.472	0.486	0.485	0.496
conn-bench-sonar-mines-rocks	208	60	2	0.497	0.487	0.509	0.536	0.537	0.555
conn-bench-vowel-deterding	990	11	11	0.672	0.466	0.365	0.683	0.559	0.471

Continued on next page.

Detecting Misclassification Errors in Neural Networks with a Gaussian Process Model

Dataset	N	M	K	RED+BNN	BNN MCP	BNN Entropy	RED+MC-D	MC-D MCP	MC-D Entropy
connect-4	67557	42	2	0.408	0.402	0.401	0.490	0.410	0.407
contrac	1473	9	3	0.634	0.629	0.622	0.605	0.599	0.594
credit-approval	690	15	2	0.388	0.359	0.365	0.414	0.402	0.409
cylinder-bands	512	35	2	0.517	0.436	0.422	0.459	0.462	0.469
dermatology	366	34	6	0.633	0.637	0.510	0.757	0.726	0.645
echocardiogram	131	10	2	0.440	0.407	0.443	0.533	0.488	0.507
ecoli	336	7	8	0.520	0.484	0.496	0.416	0.410	0.411
energy-y1	768	8	3	0.868	0.419	0.367	0.571	0.388	0.394
energy-y2	768	8	3	0.709	0.411	0.347	0.542	0.464	0.437
fertility	100	9	2	0.213	0.178	0.205	0.329	0.299	0.301
flags	194	28	8	0.794	0.750	0.746	0.764	0.718	0.728
glass	214	9	6	0.664	0.511	0.499	0.541	0.480	0.476
haberman-survival	306	3	2	0.476	0.337	0.349	0.492	0.489	0.482
hayes-roth	160	3	3	0.671	0.568	0.560	0.713	0.572	0.594
heart-cleveland	303	13	5	0.772	0.744	0.760	0.709	0.687	0.695
heart-hungarian	294	12	2	0.494	0.460	0.463	0.417	0.387	0.411
heart-switzerland	123	12	5	0.755	0.700	0.656	0.647	0.619	0.585
heart-va	200	12	5	0.833	0.812	0.828	0.753	0.715	0.733
hepatitis	155	19	2	0.610	0.559	0.585	0.616	0.582	0.564
hill-valley	1212	100	2	0.513	0.497	0.533	0.570	0.565	0.548
horse-colic	368	25	2	0.393	0.343	0.365	0.379	0.372	0.397
ilpd-indian-liver	583	9	2	0.499	0.395	0.428	0.481	0.470	0.472
image-segmentation	2310	18	7	0.543	0.372	0.371	0.533	0.456	0.406
ionosphere	351	33	2	0.367	0.316	0.448	0.436	0.360	0.394
iris	150	4	3	0.821	0.675	0.466	0.735	0.694	0.705
led-display	1000	7	10	0.577	0.566	0.521	0.574	0.571	0.523
lenses	24	4	3	0.805	0.662	0.674	0.979	0.875	0.854
letter	20000	16	26	0.461	0.455	0.401	0.705	0.627	0.563
libras	360	90	15	0.698	0.587	0.507	0.554	0.433	0.377
low-res-spect	531	100	9	0.623	0.545	0.604	0.575	0.541	0.563
lung-cancer	32	56	3	0.775	0.734	0.716	0.863	0.805	0.773
lymphography	148	18	4	0.456	0.427	0.412	0.507	0.492	0.467
magic	19020	10	2	0.358	0.354	0.356	0.358	0.350	0.353
mammographic	961	5	2	0.444	0.434	0.425	0.435	0.431	0.432
messidor	1151	19	2	0.472	0.455	0.443	0.414	0.401	0.399
miniboone	130064	50	2	0.373	0.360	0.360	0.374	0.364	0.366
molec-biol-promoter	106	57	2	0.642	0.520	0.569	0.560	0.491	0.500
molec-biol-splice	3190	60	3	0.441	0.428	0.399	0.471	0.434	0.445
monks-1	556	6	2	0.853	0.402	0.430	0.811	0.538	0.542
monks-2	601	6	2	0.896	0.389	0.429	0.527	0.416	0.427
monks-3	554	6	2	0.626	0.486	0.485	0.661	0.519	0.515
mushroom	8124	21	2	NA	NA	NA	NA	NA	NA
musk-1	476	166	2	0.651	0.481	0.549	0.454	0.421	0.382
musk-2	6598	166	2	0.540	0.389	0.447	0.456	0.351	0.406
nursery	12960	8	5	0.427	0.227	0.235	0.598	0.349	0.306
oocytes_merluccius_nucleus_4d	1022	41	2	0.813	0.487	0.470	0.407	0.387	0.387
oocytes_merluccius_states_2f	1022	25	3	0.464	0.404	0.358	0.449	0.426	0.468
oocytes_trisopterus_nucleus_2f	912	25	2	0.572	0.443	0.436	0.384	0.370	0.386
oocytes_trisopterus_states_5b	912	32	3	0.481	0.374	0.420	0.408	0.382	0.383
optical	5620	62	10	0.332	0.307	0.313	0.418	0.407	0.363
ozone	2536	72	2	0.321	0.240	0.285	0.350	0.351	0.337
page-blocks	5473	10	5	0.446	0.365	0.320	0.405	0.376	0.354
parkinsons	195	22	2	0.785	0.562	0.533	0.538	0.453	0.509
pendigits	10992	16	10	0.328	0.309	0.314	0.397	0.371	0.281
phishing	1353	9	3	0.604	0.451	0.454	0.559	0.471	0.444
pima	768	8	2	0.488	0.472	0.465	0.469	0.466	0.464
pittsburg-bridges-MATERIAL	106	7	3	0.485	0.410	0.460	0.548	0.507	0.500
pittsburg-bridges-REL-L	103	7	3	0.642	0.569	0.525	0.590	0.535	0.531
pittsburg-bridges-SPAN	92	7	3	0.593	0.579	0.622	0.545	0.498	0.520
pittsburg-bridges-T-OR-D	102	7	2	0.585	0.462	0.526	0.466	0.437	0.468
pittsburg-bridges-TYPE	105	7	6	0.834	0.758	0.755	0.784	0.725	0.720
planning	182	12	2	0.331	0.315	0.350	0.331	0.329	0.323
plant-margin	1600	64	100	0.623	0.603	0.509	0.614	0.603	0.476
plant-shape	1600	64	100	0.814	0.788	0.743	0.685	0.646	0.571
plant-texture	1599	64	100	0.659	0.650	0.556	0.654	0.624	0.503
post-operative	90	8	3	0.345	0.326	0.308	0.360	0.352	0.366
primary-tumor	330	17	15	0.880	0.854	0.845	0.809	0.803	0.801
ringnorm	7400	20	2	0.381	0.344	0.304	0.415	0.350	0.377
seeds	210	7	3	0.662	0.654	0.734	0.717	0.654	0.657
semeion	1593	256	10	0.552	0.538	0.479	0.538	0.514	0.499
soybean	683	35	18	0.555	0.522	0.393	0.534	0.519	0.410
spambase	4601	57	2	0.332	0.318	0.331	0.359	0.355	0.377
spect	265	22	2	0.473	0.427	0.418	0.518	0.513	0.518
spectf	267	44	2	0.784	0.581	0.575	0.430	0.362	0.355
statlog-australian-credit	690	14	2	0.471	0.360	0.347	0.446	0.414	0.421
statlog-german-credit	1000	24	2	0.602	0.547	0.557	0.418	0.412	0.422
statlog-heart	270	13	2	0.459	0.432	0.400	0.402	0.376	0.395

Continued on next page.

Detecting Misclassification Errors in Neural Networks with a Gaussian Process Model

Dataset	N	M	K	RED+BNN	BNN MCP	BNN Entropy	RED+MC-D	MC-D MCP	MC-D Entropy
statlog-image	2310	18	7	0.548	0.422	0.351	0.508	0.460	0.403
statlog-landsat	6435	36	6	0.491	0.457	0.447	0.445	0.415	0.380
statlog-shuttle	58000	9	7	0.541	0.284	0.448	0.669	0.447	0.483
statlog-vehicle	846	18	4	0.546	0.532	0.439	0.526	0.493	0.450
steel-plates	1941	27	7	0.605	0.539	0.481	0.546	0.516	0.491
synthetic-control	600	60	6	0.439	0.310	0.713	0.584	0.426	0.463
teaching	151	5	3	0.727	0.694	0.693	0.699	0.650	0.626
thyroid	7200	21	3	0.561	0.452	0.488	0.547	0.489	0.478
tic-tac-toe	958	9	2	0.863	0.257	0.398	0.693	0.458	0.558
titanic	2201	3	2	0.367	0.346	0.338	0.344	0.344	0.346
trains	10	29	2	1.000	0.833	0.917	0.979	0.812	0.812
twonorm	7400	20	2	0.376	0.351	0.360	0.379	0.373	0.374
vertebral-column-2classes	310	6	2	0.549	0.502	0.509	0.477	0.463	0.476
vertebral-column-3classes	310	6	3	0.679	0.632	0.599	0.476	0.472	0.472
wall-following	5456	24	4	0.427	0.379	0.372	0.439	0.396	0.413
waveform	5000	21	3	0.418	0.395	0.368	0.432	0.424	0.392
waveform-noise	5000	40	3	0.441	0.430	0.398	0.440	0.429	0.406
wine	178	13	3	0.675	0.648	0.732	0.843	0.820	0.695
wine-quality-red	1599	11	6	0.578	0.532	0.521	0.521	0.502	0.492
wine-quality-white	4898	11	7	0.509	0.497	0.475	0.510	0.503	0.477
yeast	1484	8	10	0.605	0.597	0.576	0.596	0.590	0.549
zoo	101	16	7	0.907	0.821	0.808	0.931	0.802	0.847

Continued from previous page.

Table 11: Comparison between RED and Counterparts Using AP-Success

Dataset	N	M	K	RED+BNN	BNN MCP	BNN Entropy	RED+MC-D	MC-D MCP	MC-D Entropy
abalone	4177	8	3	0.855	0.854	0.849	0.854	0.852	0.851
acute-inflammation	120	6	2	NA	NA	NA	NA	NA	NA
acute-nephritis	120	6	2	NA	NA	NA	NA	NA	NA
adult	48842	14	2	0.970	0.969	0.970	0.970	0.969	0.970
annealing	898	31	5	0.983	0.950	0.947	0.981	0.971	0.974
arrhythmia	452	262	13	0.805	0.756	0.811	0.831	0.814	0.827
audiology-std	196	59	18	0.920	0.881	0.939	0.943	0.906	0.927
balance-scale	625	4	3	0.999	0.996	0.997	0.999	0.998	0.999
balloons	16	4	2	0.869	0.845	0.845	0.880	0.861	0.861
bank	4521	16	2	0.985	0.980	0.981	0.981	0.982	0.983
bioconcentration	779	9	3	0.767	0.752	0.746	0.757	0.748	0.738
blood	748	4	2	0.903	0.885	0.905	0.902	0.903	0.905
breast-cancer	286	9	2	0.834	0.779	0.828	0.829	0.826	0.838
breast-cancer-wisc	699	9	2	0.998	0.992	0.996	0.998	0.998	0.997
breast-cancer-wisc-diag	569	30	2	0.997	0.990	0.997	0.998	0.994	0.998
breast-cancer-wisc-prog	198	33	2	0.879	0.856	0.840	0.863	0.862	0.864
breast-tissue	106	9	6	0.932	0.909	0.912	0.935	0.914	0.925
car	1728	6	4	0.997	0.998	0.998	0.999	1.000	0.999
cardiotocography-10classes	2126	21	10	0.960	0.954	0.952	0.962	0.956	0.955
cardiotocography-3classes	2126	21	3	0.990	0.988	0.989	0.992	0.991	0.992
chess-krvk	28056	6	18	0.923	0.919	0.912	0.806	0.753	0.738
chess-krvkp	3196	36	2	0.999	0.998	1.000	1.000	0.999	1.000
climate	540	20	2	0.989	0.986	0.993	0.987	0.987	0.990
congressional-voting	435	16	2	0.749	0.704	0.725	0.720	0.719	0.724
conn-bench-sonar-mines-rocks	208	60	2	0.940	0.931	0.953	0.955	0.951	0.957
conn-bench-vowel-deterding	990	11	11	0.998	0.994	0.990	0.998	0.996	0.996
connect-4	67557	42	2	0.975	0.975	0.975	0.959	0.954	0.954
contrac	1473	9	3	0.744	0.741	0.739	0.741	0.740	0.731
credit-approval	690	15	2	0.953	0.937	0.936	0.945	0.942	0.943
cylinder-bands	512	35	2	0.848	0.822	0.832	0.871	0.865	0.874
dermatology	366	34	6	0.998	0.992	0.999	1.000	1.000	0.999
echocardiogram	131	10	2	0.947	0.935	0.923	0.951	0.946	0.950
ecoli	336	7	8	0.958	0.950	0.964	0.957	0.956	0.959
energy-y1	768	8	3	0.997	0.978	0.979	0.996	0.993	0.993
energy-y2	768	8	3	0.993	0.973	0.973	0.990	0.986	0.987
fertility	100	9	2	0.959	0.923	0.928	0.962	0.935	0.939
flags	194	28	8	0.743	0.694	0.716	0.756	0.708	0.728
glass	214	9	6	0.837	0.732	0.747	0.837	0.793	0.829
haberman-survival	306	3	2	0.873	0.778	0.801	0.851	0.847	0.848
hayes-roth	160	3	3	0.974	0.969	0.963	0.955	0.904	0.905
heart-cleveland	303	13	5	0.893	0.881	0.886	0.867	0.865	0.869
heart-hungarian	294	12	2	0.934	0.913	0.929	0.926	0.908	0.911
heart-switzerland	123	12	5	0.588	0.539	0.517	0.502	0.476	0.469
heart-va	200	12	5	0.415	0.349	0.357	0.468	0.438	0.436
hepatitis	155	19	2	0.968	0.950	0.972	0.959	0.966	0.968
hill-valley	1212	100	2	0.523	0.509	0.525	0.551	0.548	0.543
horse-colic	368	25	2	0.927	0.893	0.911	0.906	0.896	0.903

Continued on next page.

Detecting Misclassification Errors in Neural Networks with a Gaussian Process Model

Dataset	N	M	K	RED+BNN	BNN MCP	BNN Entropy	RED+MC-D	MC-D MCP	MC-D Entropy
ilpd-indian-liver	583	9	2	0.873	0.845	0.853	0.880	0.876	0.876
image-segmentation	2310	18	7	0.997	0.993	0.997	0.998	0.997	0.998
ionosphere	351	33	2	0.984	0.965	0.982	0.991	0.991	0.991
iris	150	4	3	0.997	0.994	0.993	0.997	0.996	0.997
led-display	1000	7	10	0.886	0.882	0.870	0.887	0.885	0.879
lenses	24	4	3	0.893	0.820	0.832	0.990	0.945	0.935
letter	20000	16	26	0.996	0.997	0.997	0.988	0.985	0.980
libras	360	90	15	0.879	0.847	0.732	0.952	0.939	0.925
low-res-spect	531	100	9	0.973	0.966	0.979	0.979	0.974	0.984
lung-cancer	32	56	3	0.715	0.685	0.695	0.727	0.648	0.592
lymphography	148	18	4	0.950	0.933	0.943	0.932	0.936	0.934
magic	19020	10	2	0.969	0.968	0.968	0.968	0.967	0.967
mammographic	961	5	2	0.925	0.909	0.916	0.922	0.919	0.920
messidor	1151	19	2	0.812	0.809	0.810	0.872	0.871	0.870
miniboone	130064	50	2	0.993	0.992	0.993	0.992	0.992	0.993
molec-biol-promoter	106	57	2	0.934	0.838	0.908	0.928	0.901	0.901
molec-biol-splice	3190	60	3	0.978	0.976	0.975	0.970	0.969	0.972
monks-1	556	6	2	1.000	0.996	0.997	1.000	0.999	0.999
monks-2	601	6	2	0.964	0.809	0.818	0.871	0.822	0.822
monks-3	554	6	2	0.997	0.996	0.996	0.999	0.997	0.997
mushroom	8124	21	2	NA	NA	NA	NA	NA	NA
musk-1	476	166	2	0.938	0.915	0.919	0.980	0.976	0.980
musk-2	6598	166	2	0.999	0.998	0.998	1.000	0.999	1.000
nursery	12960	8	5	1.000	1.000	1.000	1.000	1.000	1.000
oocytes_merluccius_nucleus_4d	1022	41	2	0.955	0.781	0.782	0.942	0.936	0.940
oocytes_merluccius_states_2f	1022	25	3	0.987	0.983	0.985	0.991	0.988	0.991
oocytes_trisopterus_nucleus_2f	912	25	2	0.914	0.850	0.866	0.936	0.926	0.934
oocytes_trisopterus_states_5b	912	32	3	0.985	0.977	0.980	0.993	0.991	0.993
optical	5620	62	10	0.997	0.997	0.999	0.999	0.998	0.999
ozone	2536	72	2	0.996	0.993	0.995	0.995	0.993	0.996
page-blocks	5473	10	5	0.998	0.997	0.998	0.998	0.998	0.998
parkinsons	195	22	2	0.988	0.975	0.977	0.986	0.987	0.987
pendigits	10992	16	10	0.999	0.999	0.999	0.999	0.999	0.999
phishing	1353	9	3	0.974	0.967	0.967	0.979	0.976	0.974
pima	768	8	2	0.897	0.890	0.906	0.901	0.899	0.904
pittsburg-bridges-MATERIAL	106	7	3	0.978	0.963	0.971	0.976	0.973	0.973
pittsburg-bridges-REL-L	103	7	3	0.809	0.772	0.731	0.798	0.786	0.791
pittsburg-bridges-SPAN	92	7	3	0.856	0.846	0.837	0.851	0.808	0.813
pittsburg-bridges-T-OR-D	102	7	2	0.956	0.910	0.937	0.965	0.944	0.945
pittsburg-bridges-TYPE	105	7	6	0.800	0.719	0.764	0.783	0.725	0.713
planning	182	12	2	0.775	0.761	0.774	0.713	0.707	0.699
plant-margin	1600	64	100	0.935	0.934	0.909	0.954	0.952	0.919
plant-shape	1600	64	100	0.714	0.685	0.622	0.874	0.857	0.804
plant-texture	1599	64	100	0.947	0.945	0.921	0.947	0.940	0.902
post-operative	90	8	3	0.685	0.664	0.666	0.692	0.688	0.688
primary-tumor	330	17	15	0.782	0.748	0.755	0.759	0.751	0.753
ringnorm	7400	20	2	0.999	0.999	0.999	0.998	0.997	0.998
seeds	210	7	3	0.980	0.976	0.991	0.990	0.986	0.985
semeion	1593	256	10	0.992	0.991	0.992	0.992	0.993	0.993
soybean	683	35	18	0.996	0.993	0.993	0.996	0.996	0.992
spambase	4601	57	2	0.987	0.986	0.990	0.989	0.988	0.992
spect	265	22	2	0.778	0.753	0.777	0.792	0.780	0.782
spectf	267	44	2	0.965	0.951	0.955	0.959	0.949	0.950
statlog-australian-credit	690	14	2	0.744	0.669	0.664	0.721	0.705	0.705
statlog-german-credit	1000	24	2	0.904	0.899	0.900	0.892	0.897	0.899
statlog-heart	270	13	2	0.937	0.926	0.930	0.933	0.926	0.931
statlog-image	2310	18	7	0.998	0.997	0.997	0.998	0.998	0.998
statlog-landsat	6435	36	6	0.984	0.982	0.981	0.985	0.985	0.985
statlog-shuttle	58000	9	7	1.000	0.999	1.000	1.000	1.000	1.000
statlog-vehicle	846	18	4	0.944	0.940	0.914	0.970	0.967	0.965
steel-plates	1941	27	7	0.923	0.911	0.900	0.923	0.913	0.916
synthetic-control	600	60	6	0.998	0.994	1.000	1.000	0.999	0.999
teaching	151	5	3	0.616	0.580	0.548	0.709	0.648	0.640
thyroid	7200	21	3	1.000	0.999	1.000	0.999	0.999	1.000
tic-tac-toe	958	9	2	1.000	0.998	0.999	1.000	0.999	0.999
titanic	2201	3	2	0.890	0.884	0.884	0.890	0.890	0.891
trains	10	29	2	1.000	0.833	0.917	0.979	0.812	0.812
twonorm	7400	20	2	0.999	0.999	0.999	0.999	0.998	0.999
vertebral-column-2classes	310	6	2	0.976	0.962	0.967	0.976	0.975	0.977
vertebral-column-3classes	310	6	3	0.971	0.965	0.965	0.976	0.976	0.976
wall-following	5456	24	4	0.990	0.987	0.990	0.992	0.992	0.994
waveform	5000	21	3	0.973	0.970	0.970	0.973	0.973	0.972
waveform-noise	5000	40	3	0.975	0.974	0.973	0.971	0.971	0.971
wine	178	13	3	0.997	0.990	0.999	0.999	0.998	0.999
wine-quality-red	1599	11	6	0.726	0.699	0.713	0.737	0.729	0.727
wine-quality-white	4898	11	7	0.640	0.626	0.609	0.665	0.654	0.635
yeast	1484	8	10	0.724	0.719	0.717	0.749	0.744	0.721

Continued on next page.

Detecting Misclassification Errors in Neural Networks with a Gaussian Process Model

Dataset	N	M	K	RED+BNN	BNN MCP	BNN Entropy	RED+MC-D	MC-D MCP	MC-D Entropy
zoo	101	16	7	0.998	0.996	0.997	0.998	0.996	0.995

Continued from previous page.

Table 12: Comparison between RED and Counterparts Using AUPR-Error

Dataset	N	M	K	RED+BNN	BNN MCP	BNN Entropy	RED+MC-D	MC-D MCP	MC-D Entropy
abalone	4177	8	3	0.526	0.519	0.510	0.513	0.506	0.501
acute-inflammation	120	6	2	NA	NA	NA	NA	NA	NA
acute-nephritis	120	6	2	NA	NA	NA	NA	NA	NA
adult	48842	14	2	0.414	0.406	0.405	0.415	0.405	0.404
annealing	898	31	5	0.785	0.414	0.327	0.580	0.401	0.353
arrhythmia	452	262	13	0.713	0.603	0.726	0.539	0.531	0.529
audiology-std	196	59	18	0.758	0.683	0.744	0.748	0.637	0.674
balance-scale	625	4	3	0.790	0.474	0.518	0.656	0.519	0.580
balloons	16	4	2	0.752	0.744	0.744	0.801	0.759	0.759
bank	4521	16	2	0.523	0.438	0.442	0.426	0.403	0.405
bioconcentration	779	9	3	0.557	0.477	0.477	0.454	0.427	0.408
blood	748	4	2	0.505	0.457	0.485	0.429	0.428	0.430
breast-cancer	286	9	2	0.488	0.372	0.394	0.498	0.459	0.476
breast-cancer-wisc	699	9	2	0.475	0.440	0.381	0.399	0.365	0.360
breast-cancer-wisc-diag	569	30	2	0.362	0.333	0.379	0.511	0.441	0.500
breast-cancer-wisc-prog	198	33	2	0.528	0.460	0.500	0.477	0.469	0.460
breast-tissue	106	9	6	0.830	0.751	0.772	0.877	0.825	0.813
car	1728	6	4	0.591	0.475	0.316	0.628	0.418	0.277
cardiotocography-10classes	2126	21	10	0.542	0.509	0.457	0.524	0.482	0.457
cardiotocography-3classes	2126	21	3	0.490	0.413	0.409	0.458	0.388	0.392
chess-krvk	28056	6	18	0.514	0.500	0.473	0.751	0.674	0.648
chess-krvkp	3196	36	2	0.338	0.320	0.312	0.395	0.373	0.378
climate	540	20	2	0.523	0.486	0.489	0.406	0.374	0.431
congressional-voting	435	16	2	0.503	0.450	0.457	0.471	0.470	0.481
conn-bench-sonar-mines-rocks	208	60	2	0.463	0.460	0.466	0.494	0.496	0.510
conn-bench-vowel-deterding	990	11	11	0.648	0.439	0.337	0.665	0.541	0.435
connect-4	67557	42	2	0.407	0.401	0.401	0.490	0.409	0.407
contrac	1473	9	3	0.631	0.626	0.619	0.601	0.595	0.590
credit-approval	690	15	2	0.367	0.334	0.344	0.393	0.380	0.386
cylinder-bands	512	35	2	0.506	0.423	0.406	0.443	0.447	0.454
dermatology	366	34	6	0.593	0.646	0.423	0.682	0.639	0.535
echocardiogram	131	10	2	0.394	0.360	0.378	0.477	0.435	0.452
ecoli	336	7	8	0.491	0.454	0.462	0.389	0.383	0.371
energy-y1	768	8	3	0.861	0.398	0.346	0.552	0.353	0.365
energy-y2	768	8	3	0.698	0.392	0.330	0.521	0.445	0.410
fertility	100	9	2	0.156	0.125	0.165	0.270	0.253	0.256
flags	194	28	8	0.785	0.737	0.732	0.754	0.705	0.715
glass	214	9	6	0.651	0.493	0.478	0.522	0.456	0.447
haberman-survival	306	3	2	0.455	0.315	0.321	0.468	0.465	0.457
hayes-roth	160	3	3	0.638	0.518	0.520	0.686	0.535	0.555
heart-cleveland	303	13	5	0.764	0.730	0.750	0.700	0.674	0.683
heart-hungarian	294	12	2	0.463	0.431	0.437	0.387	0.356	0.380
heart-switzerland	123	12	5	0.741	0.680	0.633	0.628	0.597	0.561
heart-va	200	12	5	0.827	0.803	0.822	0.744	0.703	0.720
hepatitis	155	19	2	0.575	0.523	0.536	0.583	0.539	0.508
hill-valley	1212	100	2	0.508	0.491	0.529	0.566	0.561	0.543
horse-colic	368	25	2	0.365	0.314	0.339	0.354	0.347	0.372
ilpd-indian-liver	583	9	2	0.487	0.382	0.415	0.465	0.454	0.457
image-segmentation	2310	18	7	0.527	0.352	0.352	0.517	0.432	0.382
ionosphere	351	33	2	0.314	0.283	0.387	0.380	0.287	0.314
iris	150	4	3	0.772	0.624	0.381	0.686	0.631	0.619
led-display	1000	7	10	0.571	0.559	0.513	0.568	0.565	0.513
lenses	24	4	3	0.757	0.553	0.559	0.974	0.833	0.807
letter	20000	16	26	0.458	0.452	0.397	0.705	0.626	0.562
libras	360	90	15	0.689	0.572	0.492	0.534	0.403	0.347
low-res-spect	531	100	9	0.610	0.523	0.588	0.557	0.517	0.543
lung-cancer	32	56	3	0.730	0.686	0.663	0.840	0.768	0.725
lymphography	148	18	4	0.411	0.381	0.363	0.460	0.442	0.423
magic	19020	10	2	0.356	0.353	0.354	0.357	0.348	0.351
mammographic	961	5	2	0.432	0.420	0.409	0.419	0.415	0.417
messidor	1151	19	2	0.466	0.447	0.436	0.405	0.391	0.389
miniboone	130064	50	2	0.372	0.360	0.360	0.374	0.364	0.366
molec-biol-promoter	106	57	2	0.608	0.518	0.526	0.506	0.435	0.450
molec-biol-splice	3190	60	3	0.435	0.420	0.392	0.465	0.426	0.439
monks-1	556	6	2	0.827	0.354	0.377	0.788	0.474	0.477
monks-2	601	6	2	0.895	0.379	0.419	0.515	0.401	0.413
monks-3	554	6	2	0.596	0.446	0.446	0.627	0.468	0.462
mushroom	8124	21	2	NA	NA	NA	NA	NA	NA

Continued on next page.

Detecting Misclassification Errors in Neural Networks with a Gaussian Process Model

Dataset	N	M	K	RED+BNN	BNN MCP	BNN Entropy	RED+MC-D	MC-D MCP	MC-D Entropy
musk-1	476	166	2	0.640	0.460	0.534	0.428	0.389	0.340
musk-2	6598	166	2	0.533	0.378	0.438	0.435	0.328	0.381
nursery	12960	8	5	0.340	0.166	0.162	0.578	0.318	0.275
oocytes_merluccius_nucleus_4d	1022	41	2	0.810	0.478	0.461	0.394	0.373	0.374
oocytes_merluccius_states_2f	1022	25	3	0.445	0.387	0.339	0.426	0.402	0.446
oocytes_trisopterus_nucleus_2f	912	25	2	0.564	0.432	0.426	0.371	0.356	0.373
oocytes_trisopterus_states_5b	912	32	3	0.466	0.352	0.400	0.378	0.348	0.346
optical	5620	62	10	0.315	0.291	0.289	0.402	0.390	0.344
ozone	2536	72	2	0.303	0.221	0.265	0.330	0.336	0.311
page-blocks	5473	10	5	0.436	0.352	0.308	0.394	0.360	0.342
parkinsons	195	22	2	0.769	0.521	0.482	0.465	0.371	0.454
pendigits	10992	16	10	0.309	0.287	0.292	0.382	0.355	0.261
phishing	1353	9	3	0.596	0.437	0.440	0.551	0.457	0.434
pima	768	8	2	0.477	0.459	0.451	0.457	0.454	0.452
pittsburg-bridges-MATERIAL	106	7	3	0.415	0.318	0.379	0.496	0.450	0.435
pittsburg-bridges-REL-L	103	7	3	0.618	0.535	0.486	0.558	0.501	0.492
pittsburg-bridges-SPAN	92	7	3	0.550	0.534	0.582	0.499	0.449	0.463
pittsburg-bridges-T-OR-D	102	7	2	0.530	0.399	0.466	0.387	0.355	0.397
pittsburg-bridges-TYPE	105	7	6	0.825	0.737	0.738	0.770	0.704	0.694
planning	182	12	2	0.298	0.284	0.318	0.297	0.296	0.291
plant-margin	1600	64	100	0.619	0.597	0.502	0.610	0.598	0.469
plant-shape	1600	64	100	0.813	0.787	0.740	0.682	0.643	0.566
plant-texture	1599	64	100	0.655	0.646	0.550	0.650	0.620	0.496
post-operative	90	8	3	0.301	0.277	0.253	0.307	0.300	0.323
primary-tumor	330	17	15	0.878	0.850	0.841	0.804	0.797	0.794
ringnorm	7400	20	2	0.370	0.331	0.290	0.405	0.341	0.367
seeds	210	7	3	0.640	0.644	0.711	0.687	0.610	0.610
semeion	1593	256	10	0.543	0.527	0.465	0.523	0.496	0.483
soybean	683	35	18	0.524	0.487	0.354	0.498	0.482	0.368
spambase	4601	57	2	0.324	0.311	0.323	0.351	0.347	0.369
spect	265	22	2	0.452	0.404	0.394	0.498	0.492	0.497
spectf	267	44	2	0.775	0.560	0.545	0.396	0.322	0.314
statlog-australian-credit	690	14	2	0.460	0.350	0.335	0.435	0.403	0.409
statlog-german-credit	1000	24	2	0.595	0.540	0.547	0.407	0.400	0.412
statlog-heart	270	13	2	0.440	0.409	0.367	0.366	0.338	0.359
statlog-image	2310	18	7	0.532	0.404	0.330	0.491	0.439	0.373
statlog-landsat	6435	36	6	0.488	0.453	0.444	0.441	0.411	0.375
statlog-shuttle	58000	9	7	0.526	0.261	0.427	0.657	0.431	0.465
statlog-vehicle	846	18	4	0.536	0.522	0.426	0.513	0.478	0.437
steel-plates	1941	27	7	0.601	0.533	0.475	0.541	0.510	0.485
synthetic-control	600	60	6	0.391	0.233	0.684	0.510	0.340	0.386
teaching	151	5	3	0.710	0.672	0.673	0.680	0.632	0.605
thyroid	7200	21	3	0.552	0.439	0.473	0.536	0.476	0.461
tic-tac-toe	958	9	2	0.851	0.187	0.344	0.642	0.379	0.505
titanic	2201	3	2	0.361	0.340	0.332	0.338	0.338	0.340
trains	10	29	2	1.000	0.750	0.875	0.969	0.719	0.719
twonorm	7400	20	2	0.364	0.338	0.348	0.367	0.361	0.361
vertebral-column-2classes	310	6	2	0.523	0.465	0.475	0.440	0.422	0.434
vertebral-column-3classes	310	6	3	0.659	0.613	0.570	0.436	0.431	0.437
wall-following	5456	24	4	0.422	0.373	0.365	0.432	0.388	0.406
waveform	5000	21	3	0.414	0.391	0.363	0.428	0.419	0.387
waveform-noise	5000	40	3	0.437	0.425	0.393	0.436	0.425	0.401
wine	178	13	3	0.635	0.626	0.623	0.822	0.810	0.648
wine-quality-red	1599	11	6	0.574	0.527	0.516	0.517	0.497	0.487
wine-quality-white	4898	11	7	0.507	0.495	0.473	0.508	0.502	0.475
yeast	1484	8	10	0.602	0.594	0.573	0.592	0.586	0.544
zoo	101	16	7	0.888	0.771	0.764	0.904	0.733	0.819

Continued from previous page.

Table 13: Comparison between RED and Counterparts Using AUPR-Success

Dataset	N	M	K	RED+BNN	BNN MCP	BNN Entropy	RED+MC-D	MC-D MCP	MC-D Entropy
abalone	4177	8	3	0.855	0.853	0.849	0.853	0.852	0.851
acute-inflammation	120	6	2	NA	NA	NA	NA	NA	NA
acute-nephritis	120	6	2	NA	NA	NA	NA	NA	NA
adult	48842	14	2	0.970	0.969	0.970	0.970	0.969	0.970
annealing	898	31	5	0.983	0.951	0.947	0.981	0.972	0.974
arrhythmia	452	262	13	0.801	0.750	0.806	0.827	0.809	0.823
audiology-std	196	59	18	0.918	0.912	0.938	0.942	0.902	0.925
balance-scale	625	4	3	0.999	0.996	0.997	0.999	0.998	0.999
balloons	16	4	2	0.815	0.780	0.780	0.829	0.819	0.819
bank	4521	16	2	0.985	0.980	0.981	0.981	0.982	0.983
bioconcentration	779	9	3	0.764	0.749	0.741	0.753	0.744	0.734
blood	748	4	2	0.902	0.884	0.905	0.901	0.902	0.904

Continued on next page.

Detecting Misclassification Errors in Neural Networks with a Gaussian Process Model

Dataset	N	M	K	RED+BNN	BNN MCP	BNN Entropy	RED+MC-D	MC-D MCP	MC-D Entropy
breast-cancer	286	9	2	0.829	0.770	0.823	0.823	0.821	0.834
breast-cancer-wisc	699	9	2	0.998	0.995	0.995	0.998	0.998	0.997
breast-cancer-wisc-diag	569	30	2	0.997	0.995	0.997	0.998	0.996	0.998
breast-cancer-wisc-prog	198	33	2	0.875	0.855	0.833	0.858	0.859	0.860
breast-tissue	106	9	6	0.929	0.904	0.906	0.931	0.907	0.920
car	1728	6	4	0.997	0.998	0.998	0.999	1.000	0.999
cardiotocography-10clases	2126	21	10	0.960	0.954	0.952	0.962	0.956	0.955
cardiotocography-3clases	2126	21	3	0.990	0.988	0.989	0.992	0.991	0.992
chess-krvk	28056	6	18	0.923	0.919	0.912	0.806	0.753	0.738
chess-krvkv	3196	36	2	0.999	0.999	1.000	1.000	0.999	1.000
climate	540	20	2	0.988	0.991	0.993	0.987	0.989	0.990
congressional-voting	435	16	2	0.745	0.700	0.719	0.713	0.713	0.717
conn-bench-sonar-mines-rocks	208	60	2	0.939	0.948	0.952	0.954	0.951	0.956
conn-bench-vowel-deterding	990	11	11	0.998	0.994	0.990	0.998	0.996	0.996
connect-4	67557	42	2	0.975	0.975	0.975	0.959	0.954	0.954
contrac	1473	9	3	0.743	0.739	0.737	0.740	0.739	0.729
credit-approval	690	15	2	0.953	0.936	0.935	0.944	0.942	0.943
cylinder-bands	512	35	2	0.846	0.820	0.830	0.869	0.865	0.872
dermatology	366	34	6	0.998	0.996	0.999	1.000	1.000	0.999
echocardiogram	131	10	2	0.945	0.934	0.918	0.949	0.944	0.949
ecoli	336	7	8	0.958	0.954	0.963	0.956	0.955	0.959
energy-y1	768	8	3	0.997	0.978	0.979	0.996	0.993	0.993
energy-y2	768	8	3	0.993	0.975	0.973	0.990	0.986	0.987
fertility	100	9	2	0.957	0.917	0.921	0.960	0.928	0.933
flags	194	28	8	0.734	0.679	0.702	0.747	0.697	0.718
glass	214	9	6	0.832	0.729	0.741	0.833	0.786	0.824
haberman-survival	306	3	2	0.869	0.769	0.795	0.845	0.840	0.841
hayes-roth	160	3	3	0.973	0.969	0.962	0.954	0.901	0.903
heart-cleveland	303	13	5	0.891	0.879	0.884	0.865	0.863	0.866
heart-hungarian	294	12	2	0.933	0.913	0.927	0.924	0.904	0.908
heart-switzerland	123	12	5	0.562	0.505	0.489	0.470	0.445	0.437
heart-va	200	12	5	0.379	0.312	0.323	0.443	0.410	0.407
hepatitis	155	19	2	0.968	0.958	0.972	0.957	0.966	0.967
hill-valley	1212	100	2	0.517	0.504	0.519	0.546	0.542	0.538
horse-colic	368	25	2	0.926	0.894	0.909	0.904	0.895	0.901
ilpd-indian-liver	583	9	2	0.872	0.845	0.852	0.879	0.875	0.875
image-segmentation	2310	18	7	0.997	0.995	0.997	0.998	0.998	0.998
ionosphere	351	33	2	0.984	0.977	0.982	0.991	0.991	0.991
iris	150	4	3	0.997	0.994	0.993	0.997	0.996	0.997
led-display	1000	7	10	0.886	0.881	0.870	0.887	0.884	0.878
lenses	24	4	3	0.860	0.783	0.798	0.988	0.934	0.922
letter	20000	16	26	0.996	0.997	0.997	0.988	0.985	0.980
libras	360	90	15	0.878	0.845	0.728	0.952	0.938	0.924
low-res-spect	531	100	9	0.973	0.973	0.979	0.978	0.978	0.984
lung-cancer	32	56	3	0.645	0.613	0.628	0.666	0.582	0.519
lymphography	148	18	4	0.948	0.941	0.942	0.929	0.934	0.932
magic	19020	10	2	0.969	0.968	0.968	0.968	0.967	0.967
mammographic	961	5	2	0.924	0.908	0.915	0.921	0.918	0.919
messidor	1151	19	2	0.811	0.808	0.809	0.871	0.871	0.870
miniboone	130064	50	2	0.993	0.992	0.993	0.992	0.992	0.993
molec-biol-promoter	106	57	2	0.932	0.896	0.904	0.925	0.897	0.897
molec-biol-splice	3190	60	3	0.977	0.976	0.975	0.970	0.970	0.972
monks-1	556	6	2	0.999	0.996	0.997	1.000	0.999	0.999
monks-2	601	6	2	0.964	0.808	0.816	0.870	0.821	0.820
monks-3	554	6	2	0.997	0.996	0.996	0.999	0.997	0.997
mushroom	8124	21	2	NA	NA	NA	NA	NA	NA
musk-1	476	166	2	0.937	0.914	0.918	0.980	0.979	0.980
musk-2	6598	166	2	0.999	0.998	0.998	1.000	0.999	1.000
nursery	12960	8	5	1.000	1.000	1.000	1.000	1.000	1.000
oocytes_merluccius_nucleus_4d	1022	41	2	0.955	0.779	0.780	0.942	0.936	0.939
oocytes_merluccius_states_2f	1022	25	3	0.987	0.984	0.985	0.991	0.989	0.991
oocytes_trisopterus_nucleus_2f	912	25	2	0.914	0.849	0.866	0.936	0.925	0.933
oocytes_trisopterus_states_5b	912	32	3	0.984	0.977	0.980	0.993	0.992	0.993
optical	5620	62	10	0.997	0.998	0.999	0.999	0.998	0.999
ozone	2536	72	2	0.996	0.995	0.995	0.995	0.995	0.996
page-blocks	5473	10	5	0.998	0.997	0.998	0.998	0.998	0.998
parkinsons	195	22	2	0.988	0.976	0.977	0.985	0.987	0.987
pendigits	10992	16	10	0.999	0.999	0.999	0.999	0.999	0.999
phishing	1353	9	3	0.974	0.967	0.967	0.979	0.975	0.974
pima	768	8	2	0.896	0.889	0.906	0.900	0.898	0.903
pittsburg-bridges-MATERIAL	106	7	3	0.977	0.964	0.969	0.975	0.973	0.972
pittsburg-bridges-REL-L	103	7	3	0.798	0.756	0.709	0.784	0.771	0.775
pittsburg-bridges-SPAN	92	7	3	0.845	0.835	0.822	0.843	0.794	0.799
pittsburg-bridges-T-OR-D	102	7	2	0.954	0.913	0.933	0.964	0.941	0.940
pittsburg-bridges-TYPE	105	7	6	0.785	0.691	0.744	0.765	0.697	0.683
planning	182	12	2	0.766	0.750	0.765	0.699	0.692	0.682
plant-margin	1600	64	100	0.935	0.933	0.908	0.954	0.952	0.919

Continued on next page.

Detecting Misclassification Errors in Neural Networks with a Gaussian Process Model

Dataset	N	M	K	RED+BNN	BNN MCP	BNN Entropy	RED+MC-D	MC-D MCP	MC-D Entropy
plant-shape	1600	64	100	0.713	0.683	0.620	0.874	0.856	0.804
plant-texture	1599	64	100	0.947	0.945	0.947	0.947	0.940	0.902
post-operative	90	8	3	0.659	0.633	0.635	0.667	0.663	0.662
primary-tumor	330	17	15	0.777	0.740	0.747	0.753	0.744	0.747
ringnorm	7400	20	2	0.999	0.999	0.999	0.998	0.997	0.998
seeds	210	7	3	0.980	0.984	0.990	0.990	0.985	0.985
semeion	1593	256	10	0.992	0.992	0.992	0.992	0.993	0.993
soybean	683	35	18	0.996	0.994	0.993	0.996	0.996	0.992
spambase	4601	57	2	0.987	0.986	0.990	0.989	0.989	0.992
spect	265	22	2	0.769	0.743	0.769	0.785	0.772	0.773
spectf	267	44	2	0.965	0.956	0.954	0.958	0.951	0.949
statlog-australian-credit	690	14	2	0.739	0.663	0.659	0.716	0.700	0.700
statlog-german-credit	1000	24	2	0.904	0.899	0.899	0.891	0.897	0.898
statlog-heart	270	13	2	0.936	0.928	0.929	0.931	0.924	0.930
statlog-image	2310	18	7	0.998	0.997	0.997	0.998	0.998	0.998
statlog-landsat	6435	36	6	0.984	0.982	0.981	0.985	0.986	0.985
statlog-shuttle	58000	9	7	1.000	0.999	1.000	1.000	1.000	1.000
statlog-vehicle	846	18	4	0.944	0.940	0.914	0.970	0.967	0.964
steel-plates	1941	27	7	0.923	0.912	0.900	0.923	0.913	0.916
synthetic-control	600	60	6	0.998	0.997	1.000	1.000	0.999	0.999
teaching	151	5	3	0.589	0.555	0.517	0.694	0.627	0.618
thyroid	7200	21	3	1.000	0.999	1.000	0.999	0.999	1.000
tic-tac-toe	958	9	2	1.000	0.998	0.999	1.000	0.999	0.999
titanic	2201	3	2	0.890	0.884	0.885	0.890	0.889	0.891
trains	10	29	2	1.000	0.750	0.875	0.969	0.719	0.719
twonorm	7400	20	2	0.999	0.999	0.999	0.999	0.998	0.999
vertebral-column-2clases	310	6	2	0.975	0.964	0.967	0.976	0.975	0.977
vertebral-column-3clases	310	6	3	0.971	0.967	0.965	0.976	0.975	0.975
wall-following	5456	24	4	0.990	0.987	0.990	0.992	0.992	0.994
waveform	5000	21	3	0.973	0.970	0.970	0.973	0.973	0.972
waveform-noise	5000	40	3	0.975	0.974	0.973	0.971	0.971	0.971
wine	178	13	3	0.997	0.994	0.999	0.999	0.998	0.999
wine-quality-red	1599	11	6	0.725	0.697	0.711	0.736	0.728	0.725
wine-quality-white	4898	11	7	0.639	0.624	0.607	0.664	0.653	0.634
yeast	1484	8	10	0.721	0.716	0.715	0.747	0.741	0.718
zoo	101	16	7	0.997	0.996	0.997	0.998	0.996	0.995

Continued from previous page.

Table 14: Comparison between RED and Counterparts Using AUROC

Dataset	N	M	K	RED+BNN	BNN MCP	BNN Entropy	RED+MC-D	MC-D MCP	MC-D Entropy
abalone	4177	8	3	0.731	0.727	0.718	0.725	0.723	0.716
acute-inflammation	120	6	2	NA	NA	NA	NA	NA	NA
acute-nephritis	120	6	2	NA	NA	NA	NA	NA	NA
adult	48842	14	2	0.845	0.842	0.843	0.846	0.841	0.841
annealing	898	31	5	0.928	0.798	0.764	0.883	0.850	0.836
arrhythmia	452	262	13	0.766	0.703	0.784	0.709	0.698	0.700
audiology-std	196	59	18	0.850	0.814	0.865	0.874	0.814	0.851
balance-scale	625	4	3	0.982	0.946	0.965	0.977	0.955	0.968
balloons	16	4	2	0.762	0.714	0.714	0.778	0.722	0.722
bank	4521	16	2	0.900	0.867	0.876	0.868	0.872	0.877
bioconcentration	779	9	3	0.669	0.636	0.639	0.619	0.609	0.586
blood	748	4	2	0.757	0.723	0.753	0.731	0.731	0.735
breast-cancer	286	9	2	0.662	0.581	0.652	0.672	0.668	0.678
breast-cancer-wisc	699	9	2	0.944	0.876	0.911	0.943	0.938	0.936
breast-cancer-wisc-diag	569	30	2	0.898	0.769	0.896	0.941	0.893	0.929
breast-cancer-wisc-prog	198	33	2	0.720	0.687	0.671	0.696	0.692	0.689
breast-tissue	106	9	6	0.891	0.860	0.862	0.909	0.883	0.888
car	1728	6	4	0.964	0.956	0.942	0.977	0.977	0.965
cardiotocography-10clases	2126	21	10	0.848	0.835	0.810	0.845	0.831	0.818
cardiotocography-3clases	2126	21	3	0.912	0.896	0.901	0.913	0.905	0.910
chess-krvk	28056	6	18	0.792	0.781	0.762	0.777	0.716	0.696
chess-krvkp	3196	36	2	0.917	0.883	0.954	0.968	0.927	0.956
climate	540	20	2	0.906	0.877	0.916	0.881	0.868	0.897
congressional-voting	435	16	2	0.632	0.594	0.605	0.616	0.615	0.617
conn-bench-sonar-mines-rocks	208	60	2	0.780	0.794	0.825	0.827	0.824	0.836
conn-bench-vowel-deterding	990	11	11	0.965	0.916	0.863	0.969	0.936	0.928
connect-4	67557	42	2	0.852	0.851	0.851	0.832	0.807	0.808
contrac	1473	9	3	0.691	0.690	0.683	0.679	0.677	0.665
credit-approval	690	15	2	0.773	0.723	0.735	0.753	0.750	0.753
cylinder-bands	512	35	2	0.705	0.643	0.653	0.702	0.700	0.705
dermatology	366	34	6	0.937	0.882	0.969	0.988	0.987	0.982
echocardiogram	131	10	2	0.737	0.703	0.719	0.798	0.776	0.786
ecoli	336	7	8	0.817	0.807	0.835	0.780	0.777	0.800

Continued on next page.

Detecting Misclassification Errors in Neural Networks with a Gaussian Process Model

Dataset	N	M	K	RED+BNN	BNN MCP	BNN Entropy	RED+MC-D	MC-D MCP	MC-D Entropy
energy-y1	768	8	3	0.980	0.849	0.849	0.933	0.888	0.888
energy-y2	768	8	3	0.952	0.840	0.821	0.921	0.889	0.894
fertility	100	9	2	0.594	0.439	0.471	0.707	0.609	0.608
flags	194	28	8	0.756	0.721	0.730	0.752	0.699	0.715
glass	214	9	6	0.739	0.578	0.589	0.668	0.612	0.660
haberman-survival	306	3	2	0.712	0.544	0.559	0.700	0.699	0.703
hayes-roth	160	3	3	0.888	0.863	0.837	0.880	0.786	0.787
heart-cleveland	303	13	5	0.838	0.827	0.834	0.795	0.795	0.800
heart-hungarian	294	12	2	0.785	0.746	0.766	0.743	0.718	0.728
heart-switzerland	123	12	5	0.637	0.592	0.543	0.521	0.487	0.444
heart-va	200	12	5	0.627	0.568	0.590	0.583	0.545	0.561
hepatitis	155	19	2	0.853	0.812	0.859	0.843	0.849	0.850
hill-valley	1212	100	2	0.511	0.495	0.528	0.560	0.559	0.543
horse-colic	368	25	2	0.733	0.664	0.688	0.702	0.693	0.708
ilpd-indian-liver	583	9	2	0.723	0.655	0.671	0.723	0.716	0.717
image-segmentation	2310	18	7	0.934	0.898	0.938	0.946	0.936	0.952
ionosphere	351	33	2	0.853	0.777	0.851	0.882	0.874	0.878
iris	150	4	3	0.975	0.931	0.908	0.961	0.953	0.961
led-display	1000	7	10	0.760	0.753	0.728	0.760	0.756	0.738
lenses	24	4	3	0.798	0.667	0.702	0.979	0.885	0.865
letter	20000	16	26	0.940	0.950	0.943	0.935	0.920	0.895
libras	360	90	15	0.804	0.739	0.594	0.818	0.767	0.720
low-res-spect	531	100	9	0.873	0.859	0.885	0.862	0.853	0.885
lung-cancer	32	56	3	0.669	0.601	0.596	0.722	0.613	0.564
lymphography	148	18	4	0.770	0.741	0.742	0.767	0.758	0.748
magic	19020	10	2	0.816	0.814	0.816	0.813	0.811	0.811
mammographic	961	5	2	0.753	0.739	0.740	0.757	0.754	0.755
messidor	1151	19	2	0.661	0.655	0.648	0.691	0.689	0.686
miniboone	130064	50	2	0.906	0.903	0.904	0.905	0.904	0.905
molec-biol-promoter	106	57	2	0.803	0.676	0.745	0.779	0.720	0.713
molec-biol-splice	3190	60	3	0.858	0.853	0.845	0.851	0.839	0.849
monks-1	556	6	2	0.989	0.877	0.918	0.991	0.963	0.975
monks-2	601	6	2	0.934	0.581	0.611	0.742	0.639	0.641
monks-3	554	6	2	0.959	0.930	0.934	0.970	0.950	0.950
mushroom	8124	21	2	NA	NA	NA	NA	NA	NA
musk-1	476	166	2	0.838	0.769	0.792	0.835	0.821	0.828
musk-2	6598	166	2	0.968	0.957	0.961	0.971	0.937	0.971
nursery	12960	8	5	0.957	0.965	0.974	0.994	0.968	0.967
oocytes_merluccius_nucleus_4d	1022	41	2	0.910	0.649	0.641	0.771	0.761	0.764
oocytes_merluccius_states_2f	1022	25	3	0.891	0.873	0.872	0.902	0.892	0.905
oocytes_trisopterus_nucleus_2f	912	25	2	0.793	0.677	0.697	0.752	0.735	0.750
oocytes_trisopterus_states_5b	912	32	3	0.875	0.832	0.854	0.903	0.898	0.914
optical	5620	62	10	0.897	0.907	0.963	0.949	0.941	0.960
ozone	2536	72	2	0.899	0.866	0.882	0.889	0.872	0.909
page-blocks	5473	10	5	0.945	0.932	0.947	0.948	0.942	0.950
parkinsons	195	22	2	0.932	0.851	0.865	0.890	0.869	0.873
pendigits	10992	16	10	0.936	0.934	0.947	0.946	0.937	0.941
phishing	1353	9	3	0.884	0.841	0.840	0.876	0.863	0.855
pima	768	8	2	0.755	0.750	0.752	0.751	0.750	0.750
pittsburg-bridges-MATERIAL	106	7	3	0.839	0.775	0.797	0.833	0.816	0.813
pittsburg-bridges-REL-L	103	7	3	0.682	0.625	0.576	0.656	0.624	0.629
pittsburg-bridges-SPAN	92	7	3	0.716	0.698	0.702	0.675	0.618	0.643
pittsburg-bridges-T-OR-D	102	7	2	0.793	0.715	0.742	0.780	0.730	0.740
pittsburg-bridges-TYPE	105	7	6	0.791	0.728	0.750	0.771	0.715	0.712
planning	182	12	2	0.518	0.496	0.519	0.452	0.446	0.441
plant-margin	1600	64	100	0.835	0.829	0.767	0.855	0.850	0.768
plant-shape	1600	64	100	0.759	0.730	0.677	0.801	0.773	0.706
plant-texture	1599	64	100	0.856	0.853	0.796	0.853	0.840	0.760
post-operative	90	8	3	0.380	0.364	0.357	0.428	0.415	0.414
primary-tumor	330	17	15	0.831	0.811	0.803	0.781	0.777	0.777
ringnorm	7400	20	2	0.953	0.943	0.952	0.940	0.915	0.946
seeds	210	7	3	0.875	0.869	0.932	0.929	0.896	0.902
semeion	1593	256	10	0.916	0.915	0.903	0.913	0.917	0.914
soybean	683	35	18	0.932	0.907	0.901	0.950	0.948	0.904
spambase	4601	57	2	0.853	0.847	0.873	0.861	0.858	0.889
spect	265	22	2	0.616	0.576	0.592	0.656	0.646	0.649
spectf	267	44	2	0.895	0.845	0.848	0.777	0.751	0.744
statlog-australian-credit	690	14	2	0.628	0.502	0.490	0.582	0.557	0.561
statlog-german-credit	1000	24	2	0.793	0.781	0.786	0.717	0.720	0.722
statlog-heart	270	13	2	0.739	0.701	0.703	0.736	0.712	0.724
statlog-image	2310	18	7	0.949	0.938	0.938	0.953	0.947	0.954
statlog-landsat	6435	36	6	0.890	0.876	0.874	0.884	0.881	0.877
statlog-shuttle	58000	9	7	0.999	0.823	0.998	0.999	0.905	0.998
statlog-vehicle	846	18	4	0.829	0.818	0.741	0.861	0.857	0.837
steel-plates	1941	27	7	0.824	0.788	0.757	0.802	0.786	0.773
synthetic-control	600	60	6	0.861	0.738	0.980	0.974	0.965	0.966
teaching	151	5	3	0.656	0.618	0.614	0.690	0.624	0.611

Continued on next page.

Detecting Misclassification Errors in Neural Networks with a Gaussian Process Model

Dataset	N	M	K	RED+BNN	BNN MCP	BNN Entropy	RED+MC-D	MC-D MCP	MC-D Entropy
thyroid	7200	21	3	0.977	0.950	0.985	0.968	0.951	0.984
tic-tac-toe	958	9	2	0.990	0.875	0.961	0.985	0.951	0.975
titanic	2201	3	2	0.677	0.664	0.665	0.669	0.668	0.674
trains	10	29	2	1.000	0.667	0.833	0.958	0.625	0.625
twonorm	7400	20	2	0.958	0.956	0.957	0.950	0.945	0.955
vertebral-column-2clases	310	6	2	0.871	0.836	0.846	0.851	0.847	0.858
vertebral-column-3clases	310	6	3	0.888	0.877	0.870	0.861	0.860	0.859
wall-following	5456	24	4	0.894	0.879	0.889	0.909	0.900	0.919
waveform	5000	21	3	0.845	0.834	0.833	0.850	0.849	0.845
waveform-noise	5000	40	3	0.858	0.856	0.849	0.850	0.850	0.849
wine	178	13	3	0.923	0.857	0.976	0.979	0.949	0.954
wine-quality-red	1599	11	6	0.657	0.629	0.622	0.640	0.626	0.611
wine-quality-white	4898	11	7	0.583	0.568	0.544	0.598	0.588	0.560
yeast	1484	8	10	0.675	0.667	0.648	0.690	0.687	0.645
zoo	101	16	7	0.980	0.966	0.965	0.989	0.967	0.963

Continued from previous page.